

New quasars behind the Magellanic Clouds. II. Spectroscopic confirmation of 136 near-infrared selected candidates[★]

Valentin D. Ivanov¹, Maria-Rosa L. Cioni², Michel Dennefeld³, Richard de Grijs^{4,5,6}, Jessica E. M. Craig⁷, Jacco Th. van Loon⁷, Clara Pennock^{7,8}, Chandreyee Maitra⁹, and Frank Haberl⁹

¹ European Southern Observatory, Karl-Schwarzschild-Str. 2, D-85748 Garching bei München, Germany

² Leibniz-Institut für Astrophysik Potsdam, An der Sternwarte 16, D-14482 Potsdam, Germany

³ Institut d’Astrophysique de Paris (IAP), 98bis Bd Arago, 75014, Paris, France

⁴ School of Mathematical and Physical Sciences, Macquarie University, Balaclava Road, Sydney, NSW 2109, Australia

⁵ Astrophysics and Space Technologies Research Centre, Macquarie University, Balaclava Road, Sydney, NSW 2109, Australia

⁶ International Space Science Institute—Beijing, 1 Nanertiao, Zhongguancun, Hai Dian District, Beijing 100190, China

⁷ Lennard-Jones Laboratories, Keele University, ST5 5BG, UK

⁸ Institute for Astronomy, University of Edinburgh, Royal Observatory, Edinburgh EH9 3HJ, UK

⁹ Max-Planck-Institut für extraterrestrische Physik, Giessenbachstrasse 1, 85748 Garching, Germany

Received 2 November 1002 / Accepted 7 January 3003

ABSTRACT

Context. Quasi–stellar objects (QSOs) are a basis for an absolute reference system for astrometric studies. There is a need for creating such system behind nearby galaxies, to facilitate the measuring of the proper motions of these galaxies. However, the foreground contamination from the galaxies themselves is a problem for the QSO identification.

Aims. We search for new QSOs behind both Magellanic Clouds, the Magellanic Bridge, and the Magellanic Stream.

Methods. We identify QSO candidates with a combination of near–infrared colors and variability criteria from the public ESO Visual and Infrared Survey Telescope for Astronomy (VISTA) Magellanic Clouds (VMC) survey. We confirm their nature from broad emission lines with low-resolution optical spectroscopy.

Results. We confirmed the QSO nature of 136 objects. They are distributed as follows: 12 behind the LMC, 37 behind the SMC, 63 behind the Bridge, and 24 behind the Stream. The QSOs span a redshift range from $z\sim 0.1$ to $z\sim 2.9$. A comparison of our quasar selection with the Quia quasar catalog, based on *Gaia* low-resolution spectra, yields a selection and confirmation success rate of 6–19%, depending on whether the quality of the photometry, the magnitude ranges and the colors are considered. Our candidate list is rather incomplete, but the objects in it are likely to be confirmed as quasars with $\sim 90\%$ probability. Finally, we report a list of 3609 objects across the entire VMC survey that match our color and variability selection criteria; only 1249 of them have *Gaia* counterparts.

Conclusions. Our combined infrared color and variability criteria for QSO selection prove to be efficient – $\sim 90\%$ of the observed candidates are bona fide QSOs and allow to generate a list of new high-probability quasar candidates.

Key words. surveys – infrared: galaxies – QSOs:general – Magellanic Clouds

1. Introduction

Quasi–stellar objects (QSOs) are distant galaxies with central supermassive black holes accreting from their surroundings. They are only luminous on a scale of a few hundred parsecs, therefore they appear as point-like objects.

Quasar candidates are often selected based on optical or infrared (IR) variability (Hook et al. 1994; Carnerero et al. 2023; Treiber et al. 2023) radio emission (Gregg et al. 1996; Tuccillo et al. 2015) X-ray (Shanks et al. 1991; Waddell et al. 2023) or mid–IR colors (Lacy et al. 2004; Sajina et al. 2022). Multi-wavelength selections are also used (DiPompeo et al. 2015; Spiniello & Agnello 2019). Bona-fide QSOs are confirmed by their broad emission lines (although their absence does not imply the object is not a QSO), that also help to derive their redshifts (Vanden Berk et al. 2001). Millions of such objects are known today (Flesch 2023a,b; Storey-Fisher et al. 2023; Onken et al. 2023) and the lists continue to be updated with the latest surveys.

Quasars provide insights into the structure and evolution of galaxies and are cosmological probes of the intervening interstellar medium. They can also serve as an absolute astrometric reference frame as distant unmoving point-source objects – a necessity for measuring the small proper motions (PMs) within nearby galaxies. However, it is challenging to identify QSOs behind these galaxies because of the rich and diverse stellar content of the galaxies themselves that blur the boundaries of the stellar locus. Furthermore, the internal reddening inside the foreground galaxies modifies the QSOs’ colors, especially the optical ones.

Finding QSOs is difficult behind the nearby Magellanic Clouds system because of the foreground contamination and in particular behind the Small Magellanic Cloud (SMC), because it exhibits a notable depth and associated with it stronger source confusion (de Grijs & Bono 2015). Nevertheless, a significant number of QSOs have been identified there by studies that have specifically targeted this region (Blanco & Heathcote 1986; Dobrzycki et al. 2002, 2003a,b, 2005; Geha et al. 2003; Kozłowski & Kochanek 2009; Kozłowski et al. 2012, 2011; Véron-Cetty & Véron 2010; Kozłowski et al. 2013).

Send offprint requests to: V. Ivanov, e-mail: vivanov@eso.org

Optical searches can confuse QSOs with stars (van Loon & Sansom 2015; Pennock et al. 2022) or miss more highly obscured QSOs. Moving to radio (Pennock et al. 2021) or near- and mid-IR wavebands can help to alleviate the latter problem. This prompted us to search for QSOs in the VISTA (Visual and Infrared Survey Telescope for Astronomy; Emerson et al. 2006) Survey of the Magellanic Clouds system (VMC; Cioni et al. 2011). Until now the largest single spectroscopically confirmed sample of quasars – 758 QSOs – was an OGLE (Optical Gravitational Lensing Experiment Udalski et al. 1992) follow up by Kozłowski et al. (2013) and more recently – by the Quia survey based on the low-resolution ($R \sim 30$) *Gaia* spectra (Storey-Fisher et al. 2023). Our main goal is to increase the number of known quasars behind the Large and the Small Magellanic Clouds, aiming to improve the proper motion reference system. We reported our first results – 37 (34 new) QSOs, also spectroscopically confirmed – in Ivanov et al. (2016). This is the second paper in our series, with further spectroscopy from VLT (Very Large Telescope) and SAAO (South African Astronomical Observatory).

2. Sample selection

2.1. VMC

The VMC is an ESO public survey with a footprint of $184^{\circ 2}$ on the sky around the Large Magellanic Cloud (LMC), SMC, the Magellanic Bridge and Stream. The photometry reaches signal-to-noise $S/N \sim 10$ at $K_s = 20.3$ mag (Vega system) in three epochs in the Y and J bands, and in 12 epochs in the K_s band. More epochs are available for some tiles¹ and in the tile overlapping areas. The time series span nearly 8 years. The VMC science is diverse and includes: star formation and star formation history, galaxy structure, star clusters, various types of stars (e.g., RR Lyrae and Cepheids), proper motions, background galaxies and even distant quasars.

The VMC is carried out at VISTA – a 4.1m telescope located on Cerro Paranal, equipped with VIRCAM (VISTA InfraRed CAMera; Dalton et al. 2006) – a near-IR wide-field $\sim 1 \times 1.5^{\circ 2}$ camera. The data are reduced with the VISTA Data Flow System (VDFS; Irwin et al. 2004; Emerson et al. 2004) at the Cambridge Astronomical Survey Unit². Their photometric calibration is described in González-Fernández et al. (2018). The data products are available at the ESO Science Archive Facility³ or at the VISTA Science Archive (VSA; Cross et al. 2012)⁴.

2.2. Quasar candidate selection

Criteria to identify QSO candidates from VMC were defined by Cioni et al. (2013) from 117 known QSOs in a $(Y-J)$ versus $(J-K_s)$ color-color diagram (Fig. 1) and from their K_s -band variability, requiring that the absolute value of the light curve slope exceeds a certain limit: $|\text{Slope}| > 10^{-4} \text{ mag day}^{-1}$. The light curve slope was determined from a simple linear fit of the K_s band versus the time of observations in days and the adopted limit was based on the behavior of the same known quasars. The quasars were selected with the data available at the time of Phase 2 submission (DR6 plus some additional images, typically one per

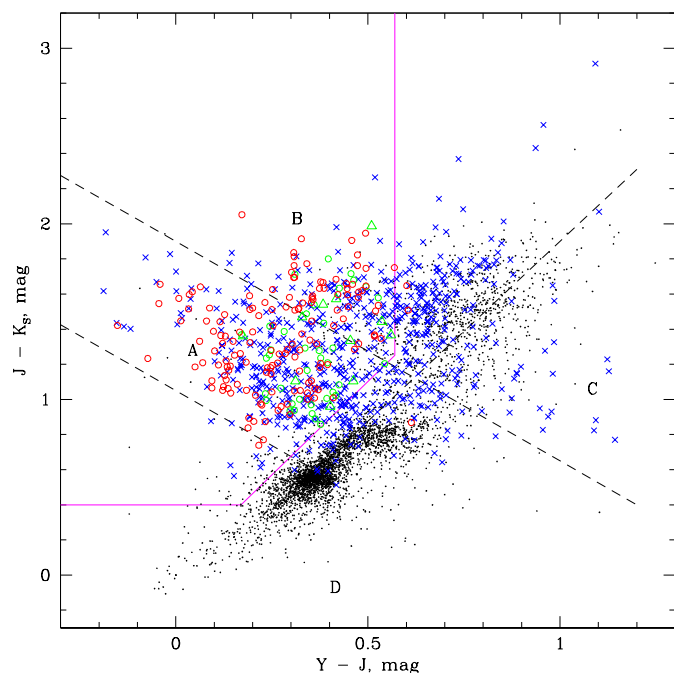


Fig. 1: Color-color diagram showing the color selection of candidates. The dashed lines identify regions (labeled with letters) with known QSOs and the solid magenta line marks the blue border of the planetary nebulae locus (Cioni et al. 2013). The confirmed QSOs from this work are red open circles. The open green circles and triangles mark QSOs and non-QSOs from Ivanov et al. (2016), respectively. Blue \times 's indicate VMC counterparts to the spectroscopically confirmed QSOs from Kozłowski et al. (2013, VMC photometry selected within a matching radius of $1''$). Black dots are randomly drawn LMC objects (with errors in all three bands < 0.1 mag) to mark the main stellar locus; some among these in regions B and C are contaminating background galaxies.

tile). Since then, some data were reprocessed and more observations became available. An inspection of updated light curves and slope measurements from them (Fig. 2) showed that a significant number of the spectroscopically confirmed quasars fall below of the adopted limit which brings up the need for adopting a more stringently defined criterion in the future, for example based on damped random walk (Kelly et al. 2009).

Here, as in Ivanov et al. (2016), we apply the same criteria on 18 tiles, mostly peripheral: 3 in LMC, 7 in SMC, 6 in the Bridge and 2 in the Stream. We selected 142 candidates: 15 in LMC, 40 in SMC, 63 in the Bridge and 24 in the Stream. The Bridge and the Stream tiles yield more candidates per tile because of the lower foreground contamination from the Magellanic Clouds and the smaller extinction. The observations were carried out under vastly diverse weather conditions because of the relaxed constraints of the program, allowing seeing of up to $2''$ and thin cloud coverage.

During the selection we excluded any previously known QSOs and gave preference to the brightest candidates in each tile, optimizing the spectroscopic follow up. Therefore, our results cannot be used to draw strict statistical conclusions. Our main goal is to confirm as many QSOs as possible for future astrometric studies.

Our main target selection was aimed at VLT follow up, but spectroscopic confirmation with smaller facilities is also possi-

¹ Tiles are contiguous images that combine six pawprints taken in an offset pattern; pawprint is an image obtained on an individual VIRCAM pointing that generates an image with gaps between the detectors. See Cioni et al. (2011) for a description of the VMC observing strategy.

² <http://casu.ast.cam.ac.uk/>

³ <http://archive.eso.org/cms.html>

⁴ <http://archive.eso.org/cms.html>

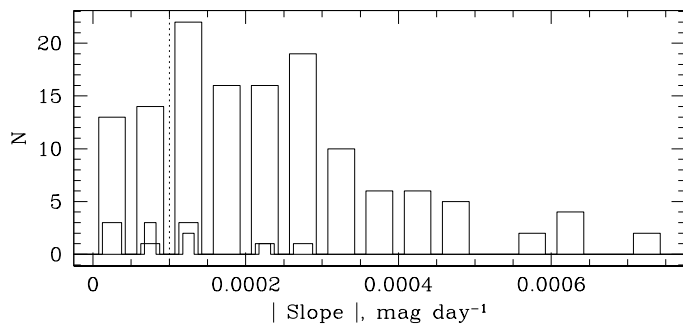


Fig. 2: Histogram of the absolute slopes from linear fit to the light curves of the objects in this paper: classified as QSOs (wide bins), remaining unknown because of poor quality spectra or lack of prominent emission lines (mid-width bins) and confirmed stars (narrow bins). The vertical dotted line is the QSO selection limit, defined by Cioni et al. (2013).

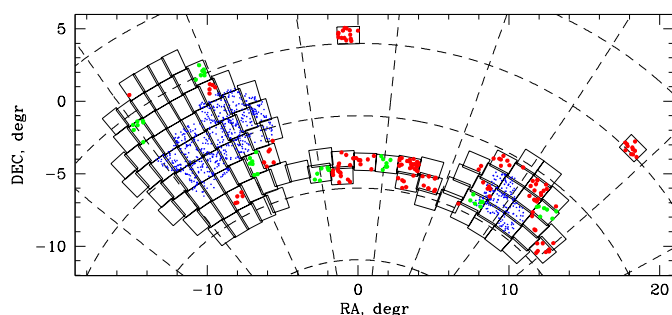


Fig. 3: Location of the spectroscopically followed up objects in this work (red) and confirmed QSOs from Kozłowski et al. (2013, blue) and Ivanov et al. (2016, green). The VMC tiles are shown as rectangles. The grid shows lines of constant right ascension and declination (spaced by 15° and 5° , respectively). Coordinates are offset with respect to $(\alpha_0, \delta_0) = (51^\circ, -69^\circ)$.

ble. To facilitate it, we performed an identical candidate selection over the entire VMC survey footprint with an additional brightness criterion of $Y < 18.0$ mag, to make possible a follow up with a 2-m class telescope. This yielded 36 objects with 15 in the range $Y = 16.5$ – 17.4 mag. Seven of these were observed, bringing the total number of followed up objects to 151.

Table 1 lists the observed candidates: the VMC identification (Col. 1), coordinates (Cols. 2–3), magnitudes in the YJK_s and their photometric errors (Cols. 4–9), and the object identification (Col. 10) used in the spectroscopic observations. The last consists of the VMC tile name and a sequential number in the catalog of sources in that tile; the letter g indicates that a source was extended according to the VDFS pipeline. Ivanov et al. (2016) demonstrated that some low redshift QSOs fall into that category. The location of the newly confirmed QSOs in the $(Y-J)$ versus $(J-K_s)$ color–color diagram is shown in Fig. 1, their positions on the sky – in Fig. 3 and their Y -band finding charts – in Fig. A.1.

Appendix B presents the complete list of all VMC survey quasar candidates in latest internal release (Aug 2022) that match our color and variability criteria, for the benefit of further studies. The color criterion alone yields 163226 objects, and 3609 of them have statistically significant slopes ($\text{Slope}/\sigma_{\text{Slope}} \geq 3$) that exceed the $|\text{Slope}| = 10^{-4}$ mag day $^{-1}$ limit.

3. Spectroscopic follow up observations

We selected for follow up 142 candidates, among the brightest in each tile and well scattered across the survey footprint to improve the chance for observing in service mode. Two additional objects (BRI 3_4 046_2 and SMC 6_3 141_2) serendipitously fell into the slits, increasing the total number of observed targets to 144. The selection and the observing followed the same procedure as in Ivanov et al. (2016). We used FORS2 (FOcal Reducer and low dispersion Spectrograph; Appenzeller et al. 1998) at the VLT (Very Large Telescope) between Oct 2016 and Aug 2017 in long-slit mode with the 300V+10 grism, GG435+81 order sorting filter, and $1.3''$ wide slit. The spectra cover $\lambda = 445$ – 865 nm with a resolving power $R = \lambda/\Delta\lambda \sim 440$. Two exposures with integration times between 60 sec and 530 seconds were taken, depending on the QSO’s apparent brightness at the time of the VMC observations, which is not necessarily the same as at the moment of the follow up because of the intrinsic QSO variability that may render the quasars fainter or brighter. In some cases we had more exposures because the conditions were too poor even for our relaxed weather constraints or the observations were interrupted because the telescopes were closed and a full set of observations was obtained on another night. We also exploited the low quality data as long as emission lines were identifiable. The signal-to-noise ratio is typically ~ 10 – 20 at the centre of the wavelength range, at continuum level and higher at the emission lines. The reduction was performed with the FORS2 pipeline (v. 5.3.23). The spectrophotometric calibration was carried out with standards (Oke 1990; Hamuy et al. 1992, 1994; Moehler et al. 2014a,b), observed and processed as the science spectra. The VLT observing log is given in Table 2.

An additional seven objects (bringing the total number of spectra to 151) were observed with SpUpNIC⁵ (Spectrograph Upgrade: Newly Improved Cassegrain; Crause et al. 2016, 2019) long slit spectrograph at the 1.9-m telescope at SAAO in Nov 2017. Grating 7 with no order separation filter (to extend the spectral coverage; emission lines from the second order spectra were ignored) was used with a $1.95''$ wide slit, delivering a resolving power of $R \sim 700$ – 1700 over $\lambda\lambda = 3750$ – 9300 Å. The slit was always oriented East-West and a single 1800 s exposure was taken for each object. The data reduction was performed in the standard way, with bias and dome flat field corrections. The wavelength calibration was done with spectra from an internal CuAr lamp, obtained after each science observation to cancel out possible instrument flexures. Feige 110 and LTT 3218 standards (from the same lists as for the VLT) were used to derive the spectral response. The 1.9-m telescope observing log is given in Table 3.

The reduced 148 spectra (for three objects no 1-dimensional spectra could be extracted, usually due to poor weather conditions) are shown in Fig. 4. The emission lines were identified by comparing our spectra with a composite QSO spectrum (Vanden Berk et al. 2001). Usually, we had multiple lines; if only one was available, it had to be MgII 2798 Å, because if the line belonged to a different element or if the redshift was different, other emission lines with comparable strength would have been inside the observed wavelength range (given that the S/N was sufficient to detect the MgII), and such lines were missing. The redshifts were measured as in Ivanov et al. (2016), fitting emission lines with Gaussian profiles using the IRAF⁶ task *splot*. The results are listed in Table 4. Some features at the edges of the spectra

⁵ <https://www.sao.ac.za/astronomers/spupnic/>

⁶ The Image Reduction and Analysis Facility is distributed by the National Optical Astronomy Observatory, which is operated by the As-

or suffering heavy contamination by sky emission lines or affected by intervening absorption were omitted from the analysis. The statistical errors and errors from wavelength calibration are negligible (see Sect. 3 in Ivanov et al. 2016). We measured the redshift error from different lines of the same object. The finding charts of followed up objects are shown in Fig. A.

A single line was observed in some spectra. For example, this occurs for quasars at redshifts between ~ 1 and ~ 1.4 when the only prominent line within our wavelength range is $\text{MgII } 2798 \text{ \AA}$. The featureless continuum outside of the line excludes the presence of any other lines: e.g., if the observed line was $\text{CIII] } 1909$, then $\text{CIV } 1549$ should have appeared in the blue part of the spectrum. In most cases the spectra have sufficient S/N (we adopt a limit of 10) at the continuum level to exclude the presence of other lines, but not always; therefore, some of our redshifts are tentative, and they are marked in Table 4 with colons signs. The table also contains the S/N calculated in the vicinity of each emission line that we used for redshift evaluation. The S/N refers to resolution elements, so for the broad lines the real S/N is much higher and especially for the redshift estimates the derived errors for the central wavelength are more relevant. For narrow line objects the estimated S/N is dominated by the continuum level and is a lower limit for core of the line (e.g., in LMC 3_5 085g, Bridge 3_4 209g, Bridge 2_7 053g). Finally, for the single line objects we tentatively assign redshift errors of 0.005 for $z \leq 1$ and 0.015 for $z > 1$ – typical values at these redshifts.

4. Results and Discussion

4.1. Quasar confirmation

The majority of the candidates – 136 out of 148 observed objects – are bona fide QSOs at $z \sim 0.1$ – 2.9 (Fig. 4). They all show some broad emission lines even though some spectra need block averaging, typically by 4 resolution bins, to make their features clearly evident on the plot (the line measurements were done on the original, not smoothed spectra). $\text{Ly}\alpha$ is visible in the spectra of the highest redshift QSOs, the rest of the sample shows other typical emission lines. The newly confirmed QSOs from the VLT observed sample are distributed as follows: 11 in LMC, 34 in SMC, 62 in the Bridge and 24 in the Stream areas; the five QSOs from the bright candidate list are: 1 in LMC, 3 in SMC and 1 in the Bridge. The spectra of six objects appear star-like with no broad emissions, and nine more are too noisy for secure classification.

The VDFS pipeline classifies 55 of our 151 objects as extended sources and 49 of these are spectroscopically confirmed QSOs. However, their extended nature seems to be more a matter of foreground contamination from Magellanic Cloud sources, rather than real resolving of the host galaxy, because 10 extended QSOs have redshift $z > 1$ and their hosts are unlikely to be resolved under atmospheric seeing conditions. Furthermore, one of the extended non-QSOs is a blue LMC star and its extended nature is likely due to a surrounding star cluster. Therefore, the VDFS classification cannot be a critical constraint when a QSO candidate sample is assembled.

Figure 5 shows that here we have a higher fraction of confirmed QSOs with $z \leq 1$ than Ivanov et al. (2016). This is likely due to the selection of brighter candidates and because this work is based on a large number of Bridge tiles where the background objects suffer less reddening and foreground contamination than

behind the LMC and SMC. Indeed, the colors of lower redshift QSOs are closer to the stellar locus than those of the higher redshift QSOs which makes them harder to identify in the inner regions of the Magellanic Clouds and easier in the Bridge.

Detections for some of our targets – all confirmed quasars – are reported in the literature: Bridge 3_4 109g and Stream 2_1 174g in UV with *GALEX* (Galaxy Evolution Explorer; Morrissey et al. 2007); SMC 4_5 060 and SMC 6_3 310 in X-ray with *XMM-Newton* (X-ray Multi-Mirror Mission; Sturm et al. 2013); SMC 6_3 310 and SMC 4_2 071g are listed as new X-ray identified active galactic nuclei candidates by Maitra et al. (2019), also based on *XMM-Newton*, and SMC 4_2 071g and again SMC 4_5 060 were detected in X-ray too, but with *Chandra* (McGowan et al. 2008). Kim et al. (2012) identified LMC 8_3 039 as a QSO candidate from a combination of light curves and multicolor criteria and our spectrum confirms it. Summarizing, only a handful of our confirmed QSOs have so far been detected in X-ray, because of the sparse coverage with sensitive observations. eROSITA, the soft X-ray instrument on board the *Spectrum-Roentgen-Gamma* (SRG) mission (Predehl et al. 2021) completely covered the region of the Magellanic Clouds during its all-sky surveys. A preliminary investigation of the eROSITA catalogue derived from the first all-sky survey data (Merloni et al. 2024) reveals a detection rate up to 30%, depending on matching criteria. More detailed work on the X-ray properties of QSOs behind the Magellanic System is in progress.

4.2. Completeness

Controlling the completeness is not a main goal of this paper – we aim to increase the number of confirmed quasars spending a minimal amount of observing time – but to estimate it nevertheless, we turn to the sample of nearly 1.3 million quasars (with $G < 20.5$ mag; Fig. 6, top panel, blue), with secure redshifts from the low-resolution *Gaia* spectra from Storey-Fisher et al. (Quaia; 2023). This catalogue suffers from its own incompleteness and contamination issues, but the spectroscopic nature of the confirmation, the large number of quasars and the full coverage of the VMC survey footprint makes it the most suitable for this purpose.

First, we determine the number of quasars that our search should find, that will also be accessible to Quaia. To compare the output of our spectroscopic confirmation campaign from this work and from Ivanov et al. (2016) with the Quaia sample we scale up our 102 VLT confirmed quasars with Quaia counterparts, with the inverse fraction of the observed tiles. Between this work and Ivanov et al. (2016) we have followed up 25 out of 110 VMC survey tiles (the seven bright additional objects followed up at the SAAO are scattered across the entire VMC survey footprint and are ignored here). Extrapolating over the entire VMC survey we scale up these 102 VLT confirmed quasars with G in the overlapping range 18–20.5 mag (to be discussed further) by an area ratio factor of 4.4, arriving at ~ 450 VMC survey quasars that we may be able to confirm, applying the same selection and following the same observing strategy (black dots on Fig. 6, top). This number must be compared with the expected number of Quaia quasars within the VMC survey footprint, over an identical magnitude interval.

On one hand, our estimates are optimistic, because the tiles in this study are located in the outermost regions in the system where the crowding and confusion are not as problematic as in the innermost regions; on the other, it is known that not all quasars are variable and would meet the variability criterion of Cioni et al. (2013). Furthermore, the observations were taken

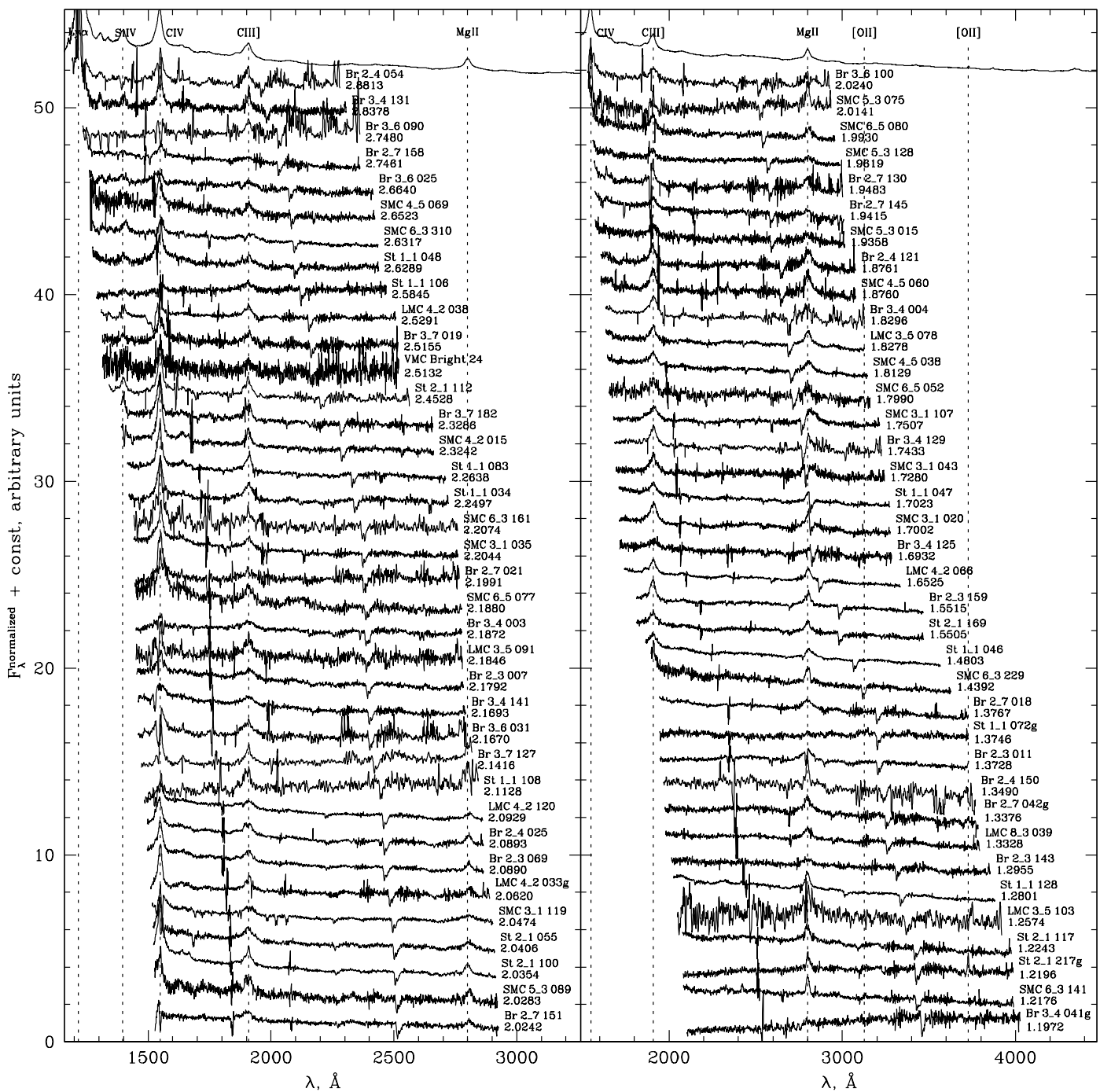


Fig. 4: Spectra of 148 objects (for three no spectra could be extracted, usually due to poor weather conditions) sorted by redshift and shifted to rest-frame wavelength. The spectra were normalized to an average value of one and shifted vertically by offsets of two, four, etc., for display purposes. The SDSS composite QSO spectrum (Vanden Berk et al. 2001) is shown at the top of all panels. Objects with no measured redshift due to lack of lines or low-S/N are plotted assuming $z=0$ in the fifth panel next to the sky spectrum to facilitate the identification of the residuals from the sky emission lines.

under highly variable weather conditions, because our program was designed as a poor weather filler and we only followed up the brightest candidates, to optimize the telescope time.

To obtain G band magnitudes for our candidates and confirmed quasars we cross-identified them with the *Gaia* DR3 main catalog (Gaia Collaboration 2022), within a radius of $0.35''$. The results for the former are reported in Table B.1, and for the latter – in the red histogram Fig. 6, top panel, for 161 objects (quasars confirmed at the 1.9-m SAAO are excluded from statistical con-

siderations). It appears 42 ($\sim 24\%$) of them can not ever have Quia counterparts because they fall below its $G=20.5$ mag limit, and the bright Quia quasars fall in the VMC saturation regime. Here and further the matching radius was set to make any spurious contamination unlikely: we repeated the cross-identification with a modified coordinates, increasing the Dec by $10'$ and found only 5 matches, three of which are with separations $>0.9''$ and the two others at $0.25\text{--}0.35''$. This keeps the spurious contamination at $\sim 0.1\%$ level.

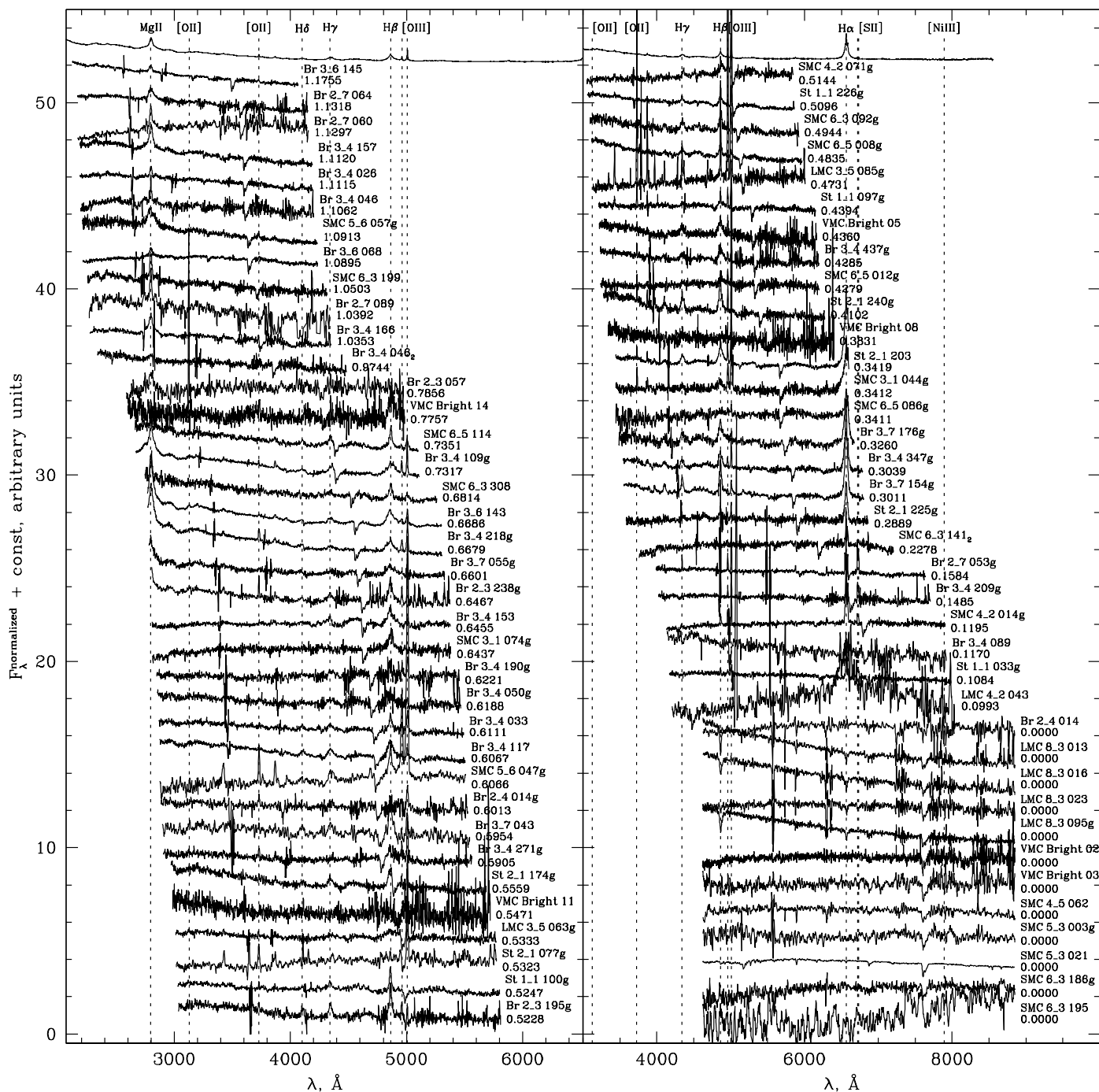


Fig. 4: Continued.

The saturation of brighter sources in the VMC is the reason why our quasars are relatively faint. Bright quasars are important for studies like those of intervening absorption lines but they constitute only a small fraction: integrating the Quiaia luminosity function above $G=16.5$ mag we find that quasars that have not a single VMC survey counterpart constitute $\sim 0.1\%$ of the entire Quiaia sample, and brighter than $G=18.0$ mag, which is the brightest limit of our confirmed quasars (black dashed line on the upper panel) – only $\sim 2.3\%$.

Second, we determine the number of Quiaia quasars that are accessible to the VMC survey based quasar search and follow up. We cross-identified Quiaia quasars with the VMC source catalog (as of DR6): 7386 Quiaia quasars fall within the VMC sur-

vey footprint; 6923 have matches within $0.35''$ radii, but only for 3149 we have photometry in all three bands of sufficiently high quality – with no contamination or error flags and errors < 0.15 mag; 2347 matches remain if our color selection criteria are applied. Here we consider all objects, regardless of their apparent G band magnitude. However, for a proper comparison we should exclude objects that are too bright and would saturate in the VMC – they would reside in the bright bin with $G < 17.5$ – 18 mag, as seen in Fig. 6. Integrating the Quiaia luminosity function above this limit indicates that only $\sim 2\%$ of Quiaia quasars are lost, so we ignore them for the purpose of this comparison.

Finally, our expected yield of 450 confirmed quasars – within the Quiaia apparent magnitude range – from the entire VMC sur-

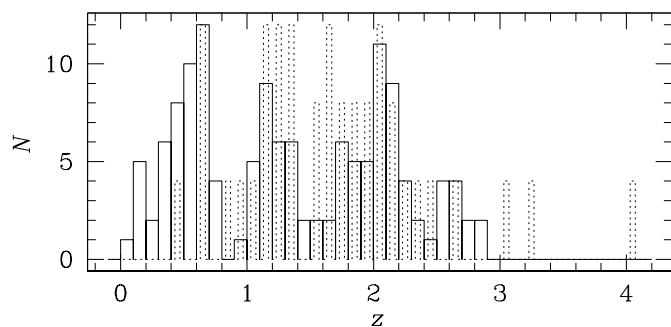


Fig. 5: Redshift histogram for 136 confirmed QSOs (solid line) and for comparison the 47 objects with measured redshift from Ivanov et al. (2016, dashed line).

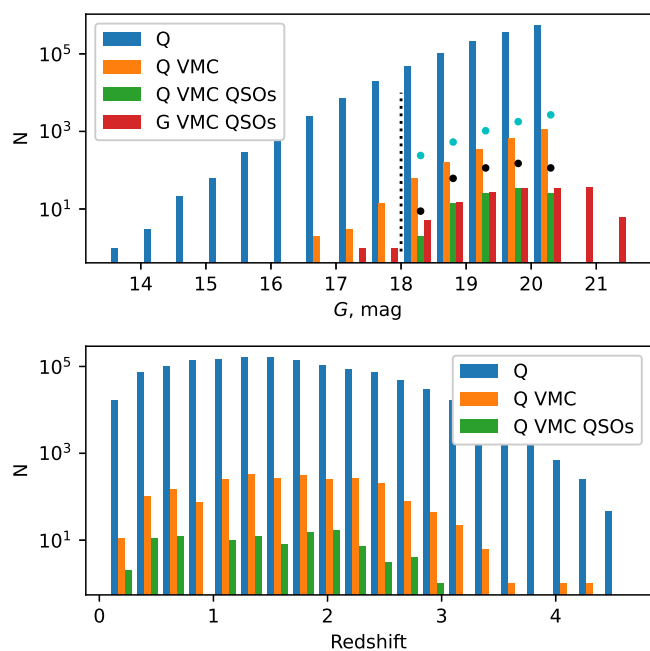


Fig. 6: *Top*: Luminosity functions of quasars from Quaia and the VMC survey in G band: blue – for all Quaia quasars (1.3 million objects); orange – Quaia quasars with VMC counterparts with quasar-like colors (2347 objects); red – spectroscopically confirmed VMC quasars from this paper and from Ivanov et al. (2016) with *Gaia* counterparts (161 objects); green – same as red, but excluding the 5 objects from the bright SAAO sample and those that fall below the Quaia $G=20.5$ mag limit; black dots – projected output for a VMC survey full quasar sample (450 objects); cyan dots – confirmed Quaia quasars scaled down from the full sky to the VMC survey area (~ 6300 objects), assuming 10% loss in the Zone of avoidance, in reality 7386 Quaia quasars fall in the VMC survey footprint. *bottom*: Redshift distribution: blue – for all Quaia quasars (1.3 million objects); orange – Quaia quasars with VMC counterparts with quasar-like colors (2347 objects); green – Quaia quasars with spectroscopically confirmed quasars from our VMC selection (161 objects). See Sect. 4 for details.

vey constitute $\sim 6\%$ of all Quaia quasars. This fraction increases to $\sim 19\%$ of nearly 2350 Quaia quasars that match our color criteria. We speculate that these low fractions come from the weak variability of most quasars, that our survey data can not recog-

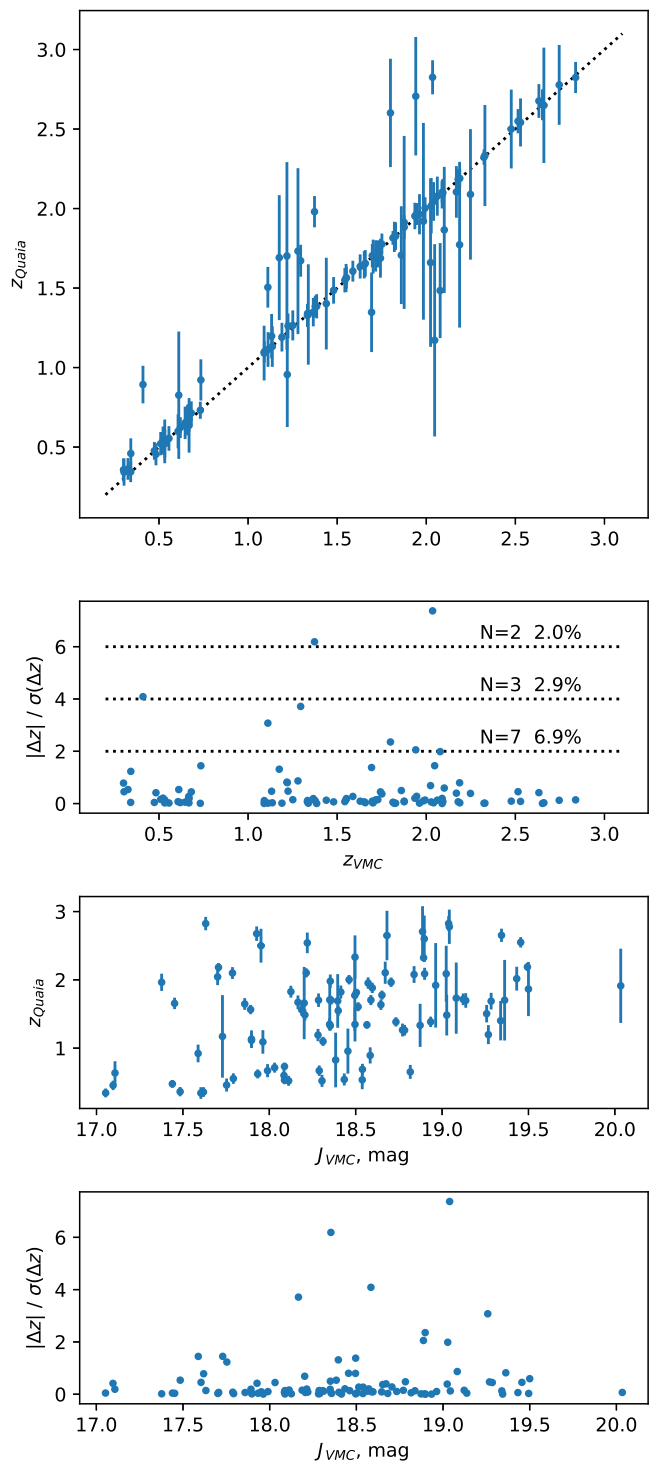


Fig. 7: Comparison of the redshifts from Quaia and from our VLT spectra (top) and absolute values of the differences as function of redshift in units of sigma (bottom). The labels above each dashed line indicate the numbers of quasars above these lines and the corresponding fractions in percentages. See Sect. 4 for details.

nize. This is consistent with our preliminary investigation of the light curves of Quaia quasars with multi-epoch counterparts in the VMC survey: it suggests that the vast majority of Quaia quasars are indeed not variable enough to meet our minimum

light curve slope criterion. This warrants further investigation and will be reported in another paper.

This result suggests that the complete list of our candidates presented in Table B.1 must contain only a small fraction of all quasars within the VMC footprint. However, the success rate of our new spectroscopic follow up is $\sim 90\%$ ($\sim 91\%$ for VLT and $\sim 71\%$ for 1.9-m), implying that nearly nine for every ten candidates in the list are likely to be confirmed as quasars, if a similar spectroscopic follow up is carried out.

The distribution of redshifts for the entire Quiaia (blue), the Quiaia quasars with VMC counterparts (orange) and our spectroscopically confirmed quasars with Quiaia counterparts (green) are shown in the lower panel of Fig. 6. Our sample is dominated by lower redshift quasars than Quiaia, probably because we tend to select for follow up the brightest candidates in each tile, minimizing the observing time per object. Storey-Fisher et al. (2023) make a considerable effort to verify the quality of their redshifts. A comparison with the redshift derived from our 102 VLT spectra suggest major disagreements occur in only a few percent of the cases (Fig. 7), lending extra credibility to the Quiaia catalog. The disagreeing redshifts are not concentrated towards the faintest objects but occur over a range of apparent magnitudes, and usually their Quiaia redshift errors are significantly larger than for other objects with similar magnitudes.

4.3. Color-redshift relations

We explored if the diagnostic color-color diagram that we use to select candidates can help to constrain their redshift. To expand the statistics we added to the VMC QSOs the QSOs from the latest catalog of Véron-Cetty & Véron (2010, 13 edition) that have been observed with some other VISTA/VIRCAM surveys: VHS (McMahon et al. 2013, 5719 objects), VIDEO (Jarvis et al. 2013, 339 objects), and VVV (Minniti et al. 2010, 5 objects). The color-color diagram coded by redshift is shown in the left panel of Fig. 8. The lowest redshift QSOs do cluster in a locus at $Y-J \sim 0.45-0.65$ mag and $J-K_S \sim 1.1-1.8$ mag, but the more distant scatter over the entire diagram. The reason for this behavior can be understood from the panels on the right that show how the two colors vary with redshift – there are sharp color changes as various more prominent emission lines enter or exit the bandpasses of individual filters. Therefore, this diagram has the potential of separating only the nearest QSOs.

5. Summary

We spectroscopically confirmed 136 QSOs within the footprint of the Magellanic system. They were selected from their near-IR colors and variability from the ESO VMC public survey. The uniform VMC observations, spanning nearly 8 yr proved a reliable resource for QSO selection, because nearly 90% of the observed candidates were quasars. However, a comparison with the Quiaia catalog indicated that our selection recovers only 6-19% of quasars identified from the *Gaia* low-resolution spectra. The fraction depends on whether the magnitude range, the quality of VMC survey photometry and the candidate colors are considered. It appears the fraction is relatively low, because most quasars are not sufficiently variable to meet our variability criterion. Therefore, our quasar candidate list is far from complete, but the candidates on it are quasars with a high degree of certainty. The variability is an important quasar identification tool, especially for radio-quiet of them. Finally, we report a list of 3609 candidates that meet our criteria, encompassing the entire

VMC survey footprint. Based on the previous statistics we expect that nearly 90% of them would be confirmed as quasars, should they be subjected to a spectroscopic follow up similar to the one described here.

Acknowledgements. This paper is based on observations made with ESO telescopes at the La Silla Paranal Observatory under program IDs 092.B-0104(A), 098.B-0229(A) and 099.B-0204(A). We have made extensive use of the SIMBAD Database at CDS (Centre de Données astronomiques) Strasbourg, the NASA/IPAC Extragalactic Database (NED) which is operated by the Jet Propulsion Laboratory, CalTech, under contract with NASA, and of the VizieR catalog access tool, CDS, Strasbourg, France. We thank Lisa Crause for efficient support at the SAAO telescope. JEMC acknowledges STFC studentship.

References

- Appenzeller, I., Fricke, K., Fürtig, W., et al. 1998, *The Messenger*, 94, 1
 Blanco, V. M. & Heathcote, S. 1986, *PASP*, 98, 635
 Carnerero, M. I., Raiteri, C. M., Rimoldini, L., et al. 2023, *A&A*, 674, A24
 Cioni, M.-R. L., Clementini, G., Girardi, L., et al. 2011, *A&A*, 527, A116
 Cioni, M.-R. L., Kamath, D., Rubele, S., et al. 2013, *A&A*, 549, A29
 Crause, L. A., Carter, D., Daniels, A., et al. 2016, in *Society of Photo-Optical Instrumentation Engineers (SPIE) Conference Series*, Vol. 9908, Ground-based and Airborne Instrumentation for Astronomy VI, ed. C. J. Evans, L. Simard, & H. Takami, 990827
 Crause, L. A., Gilbank, D., Gend, C. v., et al. 2019, *Journal of Astronomical Telescopes, Instruments, and Systems*, 5, 024007
 Cross, N. J. G., Collins, R. S., Mann, R. G., et al. 2012, *A&A*, 548, A119
 Dalton, G. B., Caldwell, M., Ward, A. K., et al. 2006, in *SPIE Conf. Ser.*, Vol. 6269, , 30
 de Grijs, R. & Bono, G. 2015, *AJ*, 149, 179
 DiPompeo, M. A., Bovy, J., Myers, A. D., & Lang, D. 2015, *MNRAS*, 452, 3124
 Dobrzycki, A., Eyer, L., Stanek, K. Z., & Macri, L. M. 2005, *A&A*, 442, 495
 Dobrzycki, A., Groot, P. J., Macri, L. M., & Stanek, K. Z. 2002, *ApJ*, 569, L15
 Dobrzycki, A., Macri, L. M., Stanek, K. Z., & Groot, P. J. 2003a, *AJ*, 125, 1330
 Dobrzycki, A., Stanek, K. Z., Macri, L. M., & Groot, P. J. 2003b, *AJ*, 126, 734
 Emerson, J., McPherson, A., & Sutherland, W. 2006, *The Messenger*, 126, 41
 Emerson, J. P., Irwin, M. J., Lewis, J., et al. 2004, in *SPIE Conf. Ser.*, Vol. 5493, , 401–410
 Flesch, E. W. 2023a, arXiv e-prints, arXiv:2308.01505
 Flesch, E. W. 2023b, arXiv e-prints, arXiv:2308.01507
 Gaia Collaboration. 2022, *VizieR Online Data Catalog: Gaia DR3 Part 1. Main source (Gaia Collaboration, 2022), VizieR On-line Data Catalog: I/355*. Originally published in: *Astron. Astrophys.*, in prep. (2022)
 Geha, M., Alcock, C., Allsman, R. A., et al. 2003, *AJ*, 125, 1
 González-Fernández, C., Hodgkin, S. T., Irwin, M. J., et al. 2018, *MNRAS*, 474, 5459
 Gregg, M. D., Becker, R. H., White, R. L., et al. 1996, *AJ*, 112, 407
 Hamuy, M., Suntzeff, N. B., Heathcote, S. R., et al. 1994, *PASP*, 106, 566
 Hamuy, M., Walker, A. R., Suntzeff, N. B., et al. 1992, *PASP*, 104, 533
 Hook, I. M., McMahon, R. G., Boyle, B. J., & Irwin, M. J. 1994, *MNRAS*, 268, 305
 Irwin, M. J., Lewis, J., Hodgkin, S., et al. 2004, in *SPIE Conf. Ser.*, Vol. 5493, , 411–422
 Ivanov, V. D., Cioni, M.-R. L., Bekki, K., et al. 2016, *A&A*, 588, A93
 Jarvis, M. J., Bonfield, D. G., Bruce, V. A., et al. 2013, *MNRAS*, 428, 1281
 Kelly, B. C., Bechtold, J., & Siemiginowska, A. 2009, *ApJ*, 698, 895
 Kim, D.-W., Protopapas, P., Trichas, M., et al. 2012, *ApJ*, 747, 107
 Kozłowski, S., Kochanek, C. S. 2009, *ApJ*, 701, 508
 Kozłowski, S., Kochanek, C. S., Jacyszyn, A. M., et al. 2012, *ApJ*, 746, 27
 Kozłowski, S., Kochanek, C. S., & Udalski, A. 2011, *ApJS*, 194, 22
 Kozłowski, S., Onken, C. A., Kochanek, C. S., et al. 2013, *ApJ*, 775, 92
 Lacy, M., Storrie-Lombardi, L. J., Sajina, A., et al. 2004, *ApJS*, 154, 166
 Maitra, C., Haberl, F., Ivanov, V. D., Cioni, M.-R. L., & van Loon, J. T. 2019, *A&A*, 622, A29
 McGowan, K. E., Coe, M. J., Schurch, M. P. E., et al. 2008, *MNRAS*, 383, 330
 McMahon, R. G., Banerji, M., Gonzalez, E., et al. 2013, *The Messenger*, 154, 35
 Merloni, A., Lamer, G., Liu, T., et al. 2024, *A&A*, 682, A34
 Minniti, D., Lucas, P. W., Emerson, J. P., et al. 2010, *New A*, 15, 433
 Moehler, S., Modigliani, A., Freudling, W., et al. 2014a, *The Messenger*, 158, 16
 Moehler, S., Modigliani, A., Freudling, W., et al. 2014b, *A&A*, 568, A9
 Morrissey, P., Conrow, T., Barlow, T. A., et al. 2007, *ApJS*, 173, 682
 Oke, J. B. 1990, *AJ*, 99, 1621
 Onken, C. A., Wolf, C., Hon, W. J., et al. 2023, *PASA*, 40, e010
 Pennock, C. M., van Loon, J. T., Anih, J. O., et al. 2022, *MNRAS*, 515, 6046
 Pennock, C. M., van Loon, J. T., Filipović, M. D., et al. 2021, *MNRAS*, 506, 3540

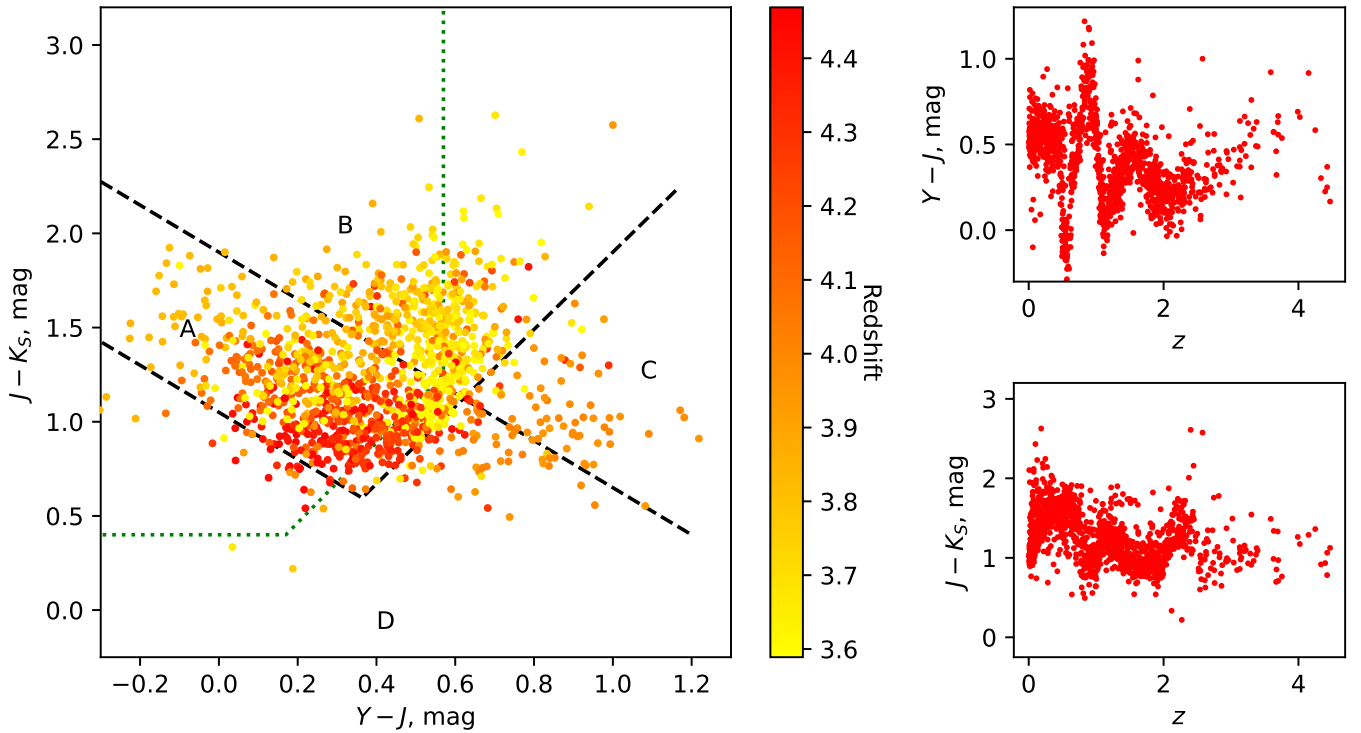


Fig. 8: *Left*: Color-color diagram of all spectroscopically confirmed QSOs with VISTA/VIRCAM photometry. For the notation of regions see Fig. 1. *Right*: $Y-J$ and $J-K_S$ colors as a function of redshift for all spectroscopically confirmed QSOs with VISTA/VIRCAM photometry. The variations are driven by strong emission lines entering and exiting the band passes of individual filters.

- Predehl, P., Andritschke, R., Arefiev, V., et al. 2021, *A&A*, 647, A1
 Sajina, A., Lacy, M., & Pope, A. 2022, *Universe*, 8, 356
 Shanks, T., Georgantopoulos, I., Stewart, G. C., et al. 1991, *Nature*, 353, 315
 Spiniello, C. & Agnello, A. 2019, *A&A*, 630, A146
 Stoehr, F., White, R., Smith, M., et al. 2008, in *Astronomical Society of the Pacific Conference Series*, Vol. 394, *Astronomical Data Analysis Software and Systems XVII*, ed. R. W. Argyle, P. S. Bunclark, & J. R. Lewis, 505
 Storey-Fisher, K., Hogg, D. W., Rix, H.-W., et al. 2023, arXiv e-prints, arXiv:2306.17749
 Sturm, R., Haberl, F., Pietsch, W., et al. 2013, *A&A*, 558, A3
 Treiber, H. P., Hinkle, J. T., Fausnaugh, M. M., et al. 2023, *MNRAS*, 525, 5795
 Tuccillo, D., González-Serrano, J. I., & Benn, C. R. 2015, *MNRAS*, 449, 2818
 Udalski, A., Szymanski, M., Kaluzny, J., Kubiak, M., & Mateo, M. 1992, *Acta Astron.*, 42, 253
 van Loon, J. T. & Sansom, A. E. 2015, *MNRAS*, 453, 2341
 Vanden Berk, D. E., Richards, G. T., Bauer, A., et al. 2001, *AJ*, 122, 549
 Véron-Cetty, M.-P. & Véron, P. 2010, *A&A*, 518, A10
 Waddell, S. G. H., Nandra, K., Buchner, J., et al. 2023, arXiv e-prints, arXiv:2306.00961

Table 1: VMC coordinates and photometry of QSO candidates (in order of increasing right ascension). The class indicates if the VDFS identified point-like (-1) or extended (1) morphology. For objects in the bright sample for the SAAO 1.9-m telescope we list (in the last column, in brackets) which tiles they fall in; more than one tile is listed for objects in overlapping regions.

VMC ID	α (h:m:s)	δ (d:m:s)	Y (mag)	σ_Y (mag)	J (mag)	σ_J (mag)	K_S (mag)	σ_{K_S} (mag)	Class	Object ID
VMC J000041.81-730258.8	00:00:41.81	-73:02:58.8	16.868	0.007	16.334	0.006	14.986	0.006	1	VMC Bright 03 (SMC 4_1)
VMC J000442.82-742013.9	00:04:42.82	-74:20:13.9	18.888	0.020	18.652	0.021	17.498	0.022	-1	SMC 3_1 107
VMC J000505.24-741051.5	00:05:05.24	-74:10:51.5	17.548	0.009	17.053	0.009	15.307	0.007	1	SMC 3_1 044g
VMC J000611.48-645423.7	00:06:11.48	-64:54:23.7	18.211	0.014	17.753	0.013	15.848	0.009	1	STR 2_1 203
VMC J000737.85-733445.6	00:07:37.85	-73:34:45.6	17.878	0.011	17.729	0.013	16.398	0.012	-1	SMC 3_1 119
VMC J000908.49-645724.4	00:09:08.49	-64:57:24.4	18.484	0.016	18.187	0.017	17.274	0.019	-1	STR 2_1 169
VMC J000953.25-644109.5	00:09:53.25	-64:41:09.5	17.884	0.012	17.701	0.013	16.489	0.013	-1	STR 2_1 055
VMC J001001.68-650200.2	00:10:01.68	-65:02:00.2	18.995	0.021	18.584	0.020	17.164	0.018	1	STR 2_1 240g
VMC J001114.13-735110.0	00:11:14.13	-73:51:10.0	18.234	0.014	17.717	0.012	16.357	0.012	1	SMC 3_1 074g
VMC J001127.76-644304.2	00:11:27.76	-64:43:04.2	18.622	0.017	18.186	0.016	16.727	0.014	1	STR 2_1 225g
VMC J001234.62-643911.8	00:12:34.62	-64:39:11.8	18.921	0.021	18.783	0.023	17.617	0.023	-1	STR 2_1 117
VMC J001400.81-641325.6	00:14:00.81	-64:13:25.6	17.800	0.011	17.792	0.013	16.217	0.011	1	STR 2_1 174g
VMC J001433.39-650655.3	00:14:33.39	-65:06:55.3	18.751	0.019	18.455	0.019	16.874	0.016	1	STR 2_1 217g
VMC J001530.24-644850.8	00:15:30.24	-64:48:50.8	19.172	0.024	19.038	0.027	17.852	0.027	-1	STR 2_1 100
VMC J001642.69-644453.8	00:16:42.69	-64:44:53.8	19.708	0.034	19.515	0.037	18.192	0.033	-1	STR 2_1 112
VMC J001809.45-644458.9	00:18:09.45	-64:44:58.9	18.494	0.016	18.538	0.020	16.992	0.017	1	STR 2_1 077g
VMC J002151.98-731723.3	00:21:51.98	-73:17:23.3	18.424	0.016	17.907	0.014	16.539	0.013	1	SMC 4_2 014g
VMC J002303.23-731801.6	00:23:03.23	-73:18:01.6	19.180	0.026	18.893	0.027	17.367	0.021	-1	SMC 4_2 015
VMC J002322.81-710941.4	00:23:22.81	-71:09:41.4	17.246	0.009	16.773	0.008	15.011	0.006	1	VMC Bright 08 (SMC 6_2)
VMC J003319.36-724305.7	00:33:19.36	-72:43:05.7	19.664	0.038	19.354	0.037	17.846	0.029	1	SMC 4_2 103
VMC J003518.92-722855.3	00:35:18.92	-72:28:55.3	17.627	0.010	17.377	0.011	16.335	0.012	-1	SMC 5_3 128
VMC J003841.18-714425.5	00:38:41.18	-71:44:25.5	19.807	0.043	19.432	0.045	18.250	0.038	-1	SMC 5_3 089
VMC J003856.59-703936.4	00:38:56.59	-70:39:36.4	19.770	0.053	19.415	0.037	17.836	0.029	-1	SMC 6_3 199
VMC J003910.78-713409.9	00:39:10.78	-71:34:09.9	16.977	0.007	16.483	0.007	14.537	0.005	-1	SMC 5_3 021
VMC J003927.58-711240.5	00:39:27.58	-71:12:40.5	19.804	0.055	19.339	0.035	18.053	0.032	-1	SMC 6_3 229
VMC J004006.53-705318.5	00:40:06.53	-70:53:18.5	18.290	0.021	17.689	0.012	16.041	0.010	1	SMC 6_3 186g
VMC J004037.07-710658.2	00:40:37.07	-71:06:58.2	20.044	0.065	19.703	0.045	17.930	0.030	-1	SMC 6_3 322
VMC J004043.60-714541.5	00:40:43.60	-71:45:41.5	19.444	0.032	19.125	0.036	17.609	0.025	-1	SMC 5_3 075
VMC J004135.79-714522.6	00:41:35.79	-71:45:22.6	18.715	0.019	18.572	0.024	17.536	0.024	-1	SMC 5_3 015
VMC J004144.30-702706.2	00:41:44.30	-70:27:06.2	18.779	0.028	18.652	0.022	17.169	0.019	1	SMC 6_3 092g
VMC J004625.33-711425.7	00:46:25.33	-71:14:25.7	20.080	0.065	19.658	0.044	18.061	0.033	-1	SMC 6_3 161
VMC J004655.15-714451.0	00:46:55.15	-71:44:51.0	19.287	0.029	18.910	0.030	17.240	0.020	1	SMC 5_3 003g
VMC J004837.07-704955.0	00:48:37.07	-70:49:55.0	19.767	0.053	19.154	0.030	18.285	0.037	-1	SMC 6_3 195
VMC J004936.13-703451.3	00:49:36.13	-70:34:51.3	18.118	0.019	17.513	0.011	16.005	0.010	1	SMC 6_3 141_2
VMC J004952.18-703231.6	00:49:52.18	-70:32:31.6	19.612	0.048	19.362	0.035	17.850	0.028	-1	SMC 6_3 141
VMC J005116.88-710857.1	00:51:16.88	-71:08:57.1	18.388	0.022	18.031	0.015	16.462	0.013	-1	SMC 6_3 308
VMC J005231.69-704705.5	00:52:31.69	-70:47:05.5	18.160	0.020	17.927	0.014	17.053	0.018	-1	SMC 6_3 310
VMC J010522.22-702251.1	01:05:22.22	-70:22:51.1	16.984	0.007	17.025	0.009	15.369	0.008	1	VMC Bright 11 (SMC 6_4, SMC 7_4)
VMC J011548.36-704338.0	01:15:48.36	-70:43:38.0	18.622	0.017	18.462	0.022	17.376	0.020	-1	SMC 6_5 080
VMC J011628.12-731447.1	01:16:28.12	-73:14:47.1	20.122	0.046	20.034	0.060	18.514	0.041	-1	SMC 4_5 060
VMC J011909.15-703106.8	01:19:09.15	-70:31:06.8	18.976	0.020	18.456	0.021	16.952	0.016	1	SMC 6_5 086g
VMC J011936.67-724616.5	01:19:36.67	-72:46:16.5	20.029	0.044	19.763	0.049	18.825	0.050	-1	SMC 4_5 062
VMC J012143.71-710205.5	01:21:43.71	-71:02:05.5	18.958	0.020	18.431	0.021	16.896	0.016	1	SMC 6_5 012g
VMC J012146.62-723949.1	01:21:46.62	-72:39:49.1	19.568	0.031	19.344	0.035	18.376	0.038	-1	SMC 4_5 069
VMC J012150.07-725023.4	01:21:50.07	-72:50:23.4	18.627	0.017	18.300	0.017	16.385	0.012	1	SMC 4_2 071g
VMC J012356.63-702107.8	01:23:56.63	-70:21:07.8	17.934	0.011	17.588	0.013	16.494	0.013	-1	SMC 6_5 114
VMC J012419.21-703931.8	01:24:19.21	-70:39:31.8	19.529	0.029	19.494	0.043	17.897	0.027	-1	SMC 6_5 077
VMC J012545.82-703925.8	01:25:45.82	-70:39:25.8	17.405	0.009	17.096	0.010	15.401	0.007	1	SMC 6_5 008g
VMC J012808.10-723547.1	01:28:08.10	-72:35:47.1	18.751	0.019	18.504	0.020	17.324	0.020	-1	SMC 4_5 038
VMC J012958.83-704859.8	01:29:58.83	-70:48:59.8	19.104	0.022	18.897	0.029	17.873	0.027	-1	SMC 6_5 052
VMC J013634.37-713838.7	01:36:34.37	-71:38:38.7	17.411	0.009	17.239	0.010	15.187	0.007	1	SMC 5_6 047g
VMC J013658.86-715542.3	01:36:58.86	-71:55:42.3	18.426	0.016	18.311	0.017	16.869	0.016	1	SMC 5_6 057g
VMC J014003.42-743845.9	01:40:03.42	-74:38:45.9	17.129	0.008	16.976	0.009	15.724	0.009	-1	VMC Bright 24 (SMC 2_5, BRI 1_2)
VMC J020706.19-741848.2	02:07:06.19	-74:18:48.2	18.514	0.019	18.434	0.020	16.988	0.017	1	BRI 2_3 195g
VMC J020721.28-742456.6	02:07:21.28	-74:24:56.6	17.874	0.012	17.706	0.014	16.445	0.013	-1	BRI 2_3 007
VMC J021022.07-733017.1	02:10:22.07	-73:30:17.1	18.730	0.022	18.353	0.020	17.147	0.019	-1	BRI 2_3 011
VMC J021044.79-733423.0	02:10:44.79	-73:34:23.0	18.414	0.018	18.166	0.017	17.020	0.017	-1	BRI 2_3 143
VMC J021335.30-742109.1	02:13:35.30	-74:21:09.1	19.169	0.028	18.816	0.026	17.263	0.020	1	BRI 2_3 238g
VMC J021353.93-742048.2	02:13:53.93	-74:20:48.2	18.235	0.016	17.892	0.015	16.891	0.016	-1	BRI 2_3 159
VMC J021644.16-733228.4	02:16:44.16	-73:32:28.4	20.532	0.081	20.344	0.078	19.506	0.086	-1	BRI 2_3 032

Table 1: Continued.

VMC ID	α (h:m:s)	δ (d:m:s)	Y (mag)	σ_Y (mag)	J (mag)	σ_J (mag)	K_S (mag)	σ_{K_S} (mag)	Class	Object ID
VMC J021905.21–741445.5	02:19:05.21	–74:14:45.5	18.336	0.017	18.214	0.018	16.894	0.016	–1	BRI 2_3 069
VMC J022232.59–733827.9	02:22:32.59	–73:38:27.9	18.808	0.044	18.592	0.054	17.853	0.037	–1	BRI 2_3 057
VMC J022822.54–732303.1	02:28:22.54	–73:23:03.1	18.118	0.012	18.085	0.016	16.570	0.014	–1	BRI 3_4 117
VMC J022842.84–725447.9	02:28:42.84	–72:54:47.9	18.813	0.019	18.671	0.023	17.481	0.022	–1	BRI 3_4 141
VMC J022923.80–731952.1	02:29:23.80	–73:19:52.1	18.573	0.016	18.088	0.016	16.468	0.013	1	BRI 3_4 109g
VMC J022941.30–724805.0	02:29:41.30	–72:48:05.0	18.974	0.021	18.579	0.022	17.381	0.021	1	BRI 3_4 209g
VMC J022955.38–730447.6	02:29:55.38	–73:04:47.6	18.849	0.019	18.496	0.020	17.390	0.021	–1	BRI 3_4 125
VMC J023009.38–730346.1	02:30:09.38	–73:03:46.1	17.922	0.011	17.632	0.012	16.659	0.014	–1	BRI 3_4 131
VMC J023043.89–724536.2	02:30:43.89	–72:45:36.2	19.415	0.028	19.284	0.034	18.173	0.035	–1	BRI 3_4 129
VMC J023108.46–734439.3	02:31:08.46	–73:44:39.3	20.091	0.045	19.737	0.043	18.291	0.037	–1	BRI 2_4 054
VMC J023121.22–731654.4	02:31:21.22	–73:16:54.4	20.547	0.062	20.101	0.062	18.470	0.042	–1	BRI 3_4 089
VMC J023243.92–725711.6	02:32:43.92	–72:57:11.6	19.542	0.030	19.441	0.039	18.165	0.034	–1	BRI 3_4 046
VMC J023225.48–725915.6	02:32:25.48	–72:59:15.6	18.388	0.015	18.129	0.016	17.635	0.025	–1	BRI 3_4 046_2
VMC J023421.27–731116.5	02:34:21.27	–73:11:16.5	18.978	0.021	18.503	0.020	16.922	0.016	1	BRI 3_4 041g
VMC J023422.51–723648.4	02:34:22.51	–72:36:48.4	19.162	0.023	18.776	0.025	17.143	0.018	–1	BRI 3_4 190g
VMC J023448.42–725828.5	02:34:48.42	–72:58:28.5	17.407	0.009	17.099	0.009	15.337	0.007	–1	BRI 3_4 153
VMC J023528.23–730158.2	02:35:28.23	–73:01:58.2	17.910	0.011	17.897	0.014	16.450	0.013	–1	BRI 3_4 157
VMC J023539.49–743705.2	02:35:39.49	–74:37:05.2	19.016	0.021	18.899	0.024	17.535	0.023	–1	BRI 2_4 025
VMC J023550.79–731710.4	02:35:50.79	–73:17:10.4	20.043	0.043	19.594	0.042	18.067	0.032	–1	BRI 3_4 166
VMC J023716.56–725030.7	02:37:16.56	–72:50:30.7	18.661	0.017	18.495	0.020	17.112	0.018	–1	BRI 3_4 003
VMC J023728.54–724242.6	02:37:28.54	–72:42:42.6	20.328	0.054	20.197	0.068	18.978	0.059	–1	BRI 3_4 004
VMC J023904.89–741504.2	02:39:04.89	–74:15:04.2	18.723	0.018	18.596	0.020	17.460	0.022	–1	BRI 2_4 121
VMC J023919.57–744321.5	02:39:19.57	–74:43:21.5	19.248	0.024	18.996	0.026	17.370	0.021	1	BRI 2_4 014g
VMC J023937.56–724942.3	02:39:37.56	–72:49:42.3	19.328	0.026	19.258	0.034	18.049	0.031	–1	BRI 3_4 026
VMC J024049.48–741133.4	02:40:49.48	–74:11:33.4	20.794	0.077	20.504	0.078	19.220	0.070	–1	BRI 2_4 150
VMC J024401.00–730831.2	02:44:01.00	–73:08:31.2	19.342	0.026	18.922	0.027	17.414	0.022	1	BRI 3_4 437g
VMC J024458.46–740624.4	02:44:58.46	–74:06:24.4	20.675	0.072	20.447	0.076	19.677	0.101	–1	BRI 2_4 014
VMC J024501.04–724116.8	02:45:01.04	–72:41:16.8	18.672	0.018	18.289	0.018	16.623	0.014	1	BRI 3_4 218g
VMC J024541.60–731211.8	02:45:41.60	–73:12:11.8	18.064	0.012	17.604	0.012	15.948	0.010	1	BRI 3_4 347g
VMC J024555.70–731435.5	02:45:55.70	–73:14:35.5	19.140	0.023	19.097	0.030	17.484	0.022	1	BRI 3_4 271g
VMC J024634.70–724504.3	02:46:34.70	–72:45:04.3	19.165	0.024	18.835	0.026	17.286	0.020	1	BRI 3_4 050g
VMC J024635.48–725142.5	02:46:35.48	–72:51:42.5	18.311	0.014	18.384	0.019	17.151	0.019	–1	BRI 3_4 033
VMC J030948.59–724423.3	03:09:48.59	–72:44:23.3	18.884	0.022	18.681	0.021	17.806	0.027	–1	BRI 3_6 025
VMC J031128.66–734010.5	03:11:28.66	–73:40:10.5	19.487	0.032	19.113	0.029	17.481	0.023	–1	BRI 3_6 031
VMC J031509.77–730025.0	03:15:09.77	–73:00:25.0	18.163	0.014	17.963	0.014	16.579	0.014	–1	BRI 3_6 068
VMC J032143.49–732110.9	03:21:43.49	–73:21:10.9	17.415	0.009	17.107	0.009	15.294	0.007	–1	BRI 3_6 143
VMC J032158.17–730440.4	03:21:58.17	–73:04:40.4	18.490	0.017	18.396	0.018	17.331	0.020	–1	BRI 3_6 145
VMC J032328.65–730310.9	03:23:28.65	–73:03:10.9	20.128	0.053	19.559	0.038	17.808	0.027	–1	BRI 3_6 090
VMC J032404.61–640722.3	03:24:04.61	–64:07:22.3	18.241	0.014	18.112	0.017	16.752	0.015	1	STR 1_1 226g
VMC J032550.80–725506.3	03:25:50.80	–72:55:06.3	19.546	0.034	19.281	0.032	18.074	0.032	–1	BRI 3_6 100
VMC J032812.35–645019.1	03:28:12.35	–64:50:19.1	18.853	0.020	18.492	0.021	17.484	0.022	1	STR 1_1 033g
VMC J032812.54–725541.5	03:28:12.54	–72:55:41.5	19.090	0.024	19.242	0.040	17.821	0.028	–1	BRI 3_7 043
VMC J032818.72–725633.6	03:28:18.72	–72:56:33.6	18.434	0.016	17.990	0.018	16.331	0.012	1	BRI 3_7 055g
VMC J032832.83–644055.8	03:28:32.83	–64:40:55.8	18.872	0.021	18.550	0.022	17.388	0.021	–1	STR 1_1 106
VMC J032850.47–642418.4	03:28:50.47	–64:24:18.4	19.939	0.042	19.619	0.045	18.102	0.033	–1	STR 1_1 108
VMC J032903.37–640515.7	03:29:03.37	–64:05:15.7	19.285	0.027	19.032	0.030	17.612	0.025	–1	STR 1_1 034
VMC J033054.45–635727.3	03:30:54.45	–63:57:27.3	18.880	0.021	18.404	0.019	16.793	0.015	1	STR 1_1 097g
VMC J033121.11–644637.6	03:31:21.11	–64:46:37.6	19.132	0.024	19.082	0.029	17.897	0.028	–1	STR 1_1 128
VMC J033126.71–732415.3	03:31:26.71	–73:24:15.3	20.131	0.049	19.830	0.063	18.106	0.033	–1	BRI 3_7 127
VMC J033206.62–743318.7	03:32:06.62	–74:33:18.7	20.603	0.065	20.275	0.070	18.902	0.059	–1	BRI 2_7 089
VMC J033207.40–635514.5	03:32:07.40	–63:55:14.5	18.288	0.015	18.088	0.016	16.568	0.014	1	STR 1_1 100g
VMC J033227.01–643655.8	03:32:27.01	–64:36:55.8	19.426	0.029	19.210	0.034	17.733	0.026	–1	STR 1_1 083
VMC J033315.61–640607.8	03:33:15.61	–64:06:07.8	18.783	0.020	18.336	0.019	16.741	0.015	1	STR 1_1 072g
VMC J033405.15–742400.3	03:34:05.15	–74:24:00.3	19.983	0.040	19.921	0.052	18.590	0.046	–1	BRI 2_7 130
VMC J033412.54–643623.8	03:34:12.54	–64:36:23.8	16.577	0.006	16.267	0.006	15.025	0.006	–1	VMC Bright 05 (STR 2_1)
VMC J033438.94–724116.9	03:34:38.94	–72:41:16.9	18.765	0.020	18.496	0.024	17.237	0.019	–1	BRI 3_7 182
VMC J033603.89–641431.8	03:36:03.89	–64:14:31.8	18.577	0.017	18.206	0.018	17.151	0.019	–1	STR 1_1 046
VMC J033611.01–642017.6	03:36:11.01	–64:20:17.6	19.659	0.035	19.421	0.040	18.241	0.036	–1	STR 1_1 048
VMC J033613.21–643309.8	03:36:13.21	–64:33:09.8	19.480	0.031	19.137	0.032	18.100	0.033	–1	STR 1_1 047
VMC J033836.66–723001.7	03:38:36.66	–72:30:01.7	18.036	0.013	17.619	0.014	15.935	0.010	1	BRI 3_7 154g
VMC J034040.77–740750.1	03:40:40.77	–74:07:50.1	18.998	0.021	18.887	0.025	17.691	0.025	–1	BRI 2_7 145
VMC J034052.05–735436.6	03:40:52.05	–73:54:36.6	19.100	0.023	18.733	0.023	17.417	0.022	–1	BRI 2_7 018
VMC J034123.04–735156.7	03:41:23.04	–73:51:56.7	17.538	0.009	17.062	0.009	15.745	0.009	1	BRI 2_7 053g
VMC J034129.52–731500.8	03:41:29.52	–73:15:00.8	17.979	0.013	17.484	0.013	15.838	0.009	1	BRI 3_7 176g

Table 1: Continued.

VMC ID	α (h:m:s)	δ (d:m:s)	Y (mag)	σ_Y (mag)	J (mag)	σ_J (mag)	K_S (mag)	σ_{K_S} (mag)	Class	Object ID
VMC J034215.07-732514.7	03:42:15.07	-73:25:14.7	19.591	0.033	19.455	0.047	18.393	0.039	-1	BRI 3_7 019
VMC J034250.73-743335.9	03:42:50.73	-74:33:35.9	19.856	0.037	19.383	0.035	17.560	0.023	-1	BRI 2_7 021
VMC J034257.34-734609.6	03:42:57.34	-73:46:09.6	19.117	0.022	18.925	0.025	17.335	0.021	-1	BRI 2_7 060
VMC J034302.85-733814.7	03:43:02.85	-73:38:14.7	19.366	0.027	19.268	0.032	17.880	0.029	-1	BRI 2_7 064
VMC J034743.46-734119.0	03:47:43.46	-73:41:19.0	19.263	0.025	19.042	0.028	18.067	0.032	-1	BRI 2_7 158
VMC J034806.80-740039.4	03:48:06.80	-74:00:39.4	18.525	0.016	18.202	0.016	16.921	0.016	-1	BRI 2_7 151
VMC J034817.21-735138.3	03:48:17.21	-73:51:38.3	19.182	0.024	18.873	0.025	17.825	0.028	1	BRI 2_7 042g
VMC J043425.74-705453.8	04:34:25.74	-70:54:53.8	17.107	0.008	16.751	0.008	15.162	0.007	1	VMC Bright 14 (LMC 5_1)
VMC J043854.34-712613.3	04:38:54.34	-71:26:13.3	18.220	0.013	17.858	0.017	16.797	0.016	-1	LMC 4_2 066
VMC J043914.87-722124.0	04:39:14.87	-72:21:24.0	18.468	0.016	18.220	0.021	16.941	0.017	-1	LMC 4_2 038
VMC J044015.31-713128.8	04:40:15.31	-71:31:28.8	20.144	0.049	19.870	0.071	18.911	0.062	-1	LMC 4_2 043
VMC J044616.30-722827.2	04:46:16.30	-72:28:27.2	17.881	0.011	17.787	0.016	16.681	0.015	-1	LMC 4_2 120
VMC J044713.31-720908.1	04:47:13.31	-72:09:08.1	18.962	0.021	18.838	0.032	17.765	0.028	1	LMC 4_2 033g
VMC J050031.54-660908.4	05:00:31.54	-66:09:08.4	20.447	0.081	20.257	0.111	19.364	0.090	-1	LMC 8_3 013
VMC J050132.72-655606.2	05:01:32.72	-65:56:06.2	18.638	0.019	18.353	0.024	17.092	0.018	-1	LMC 8_3 039
VMC J050258.90-654815.7	05:02:58.90	-65:48:15.7	20.546	0.089	20.197	0.105	18.859	0.062	-1	LMC 8_3 023
VMC J050431.38-660723.7	05:04:31.38	-66:07:23.7	19.379	0.034	19.076	0.041	17.761	0.028	1	LMC 8_3 095g
VMC J050546.58-662327.4	05:05:46.58	-66:23:27.4	20.455	0.081	20.204	0.106	19.011	0.067	-1	LMC 8_3 016
VMC J051713.17-732818.9	05:17:13.17	-73:28:18.9	20.040	0.059	19.847	0.063	18.335	0.040	-1	LMC 3_5 091
VMC J051754.32-734354.1	05:17:54.32	-73:43:54.1	18.795	0.024	18.488	0.023	16.652	0.015	1	LMC 3_5 085g
VMC J052234.44-733523.7	05:22:34.44	-73:35:23.7	18.247	0.017	18.125	0.018	17.073	0.018	-1	LMC 3_5 078
VMC J052541.50-735734.3	05:25:41.50	-73:57:34.3	18.369	0.018	18.305	0.020	16.664	0.014	1	LMC 3_5 063g
VMC J052727.83-735609.9	05:27:27.83	-73:56:09.9	20.539	0.089	20.232	0.083	18.538	0.046	-1	LMC 3_5 103
VMC J055137.33-635018.9	05:51:37.33	-63:50:18.9	16.548	0.006	16.138	0.006	15.129	0.007	1	VMC Bright 02 (LMC 10_7)
VMC J235716.69-733833.0	23:57:16.69	-73:38:33.0	18.681	0.018	18.357	0.018	17.306	0.020	-1	SMC 3_1 020
VMC J235836.89-733253.8	23:58:36.89	-73:32:53.8	19.888	0.040	19.656	0.043	18.104	0.032	-1	SMC 3_1 035
VMC J235848.46-734953.6	23:58:48.46	-73:49:53.6	19.306	0.026	19.122	0.030	18.070	0.032	-1	SMC 3_1 043

Table 2: Log of the VLT spectroscopic observations. Starting times, exposure times, starting and ending airmasses, and slit position angles for each exposure are listed on separate successive lines. Multiple exposures of each object are entered separately. Only the observations of the first three objects are shown for guidance, the entire table is included on the electronic edition.

Object ID	UT at start of obs. yyyy-mm-ddThh:mm:ss	Exp. (s)	sec z (dex)	Slit PA (deg)
BRI2_3 007	2016-12-08T05:42:13.371	60	1.912–1.916	–65.199
BRI2_3 007	2016-12-08T05:43:58.280	60	1.920–1.923	–65.199
BRI2_3 011	2016-12-05T00:26:16.593	180	1.562–1.558	30.072
BRI2_3 011	2016-12-05T00:30:04.451	180	1.559–1.556	30.072
BRI2_3 032	2016-12-07T06:00:32.486	510	1.913–1.945	–67.766
BRI2_3 032	2016-12-07T06:10:01.053	510	1.950–1.984	–67.766

Table 3: Log of the 1.9-m SAAO spectroscopic observations. Starting times and the airmasses at the start of each exposure are listed. A single 1800 sec exposure was obtained for each object.

Object ID	UT at start of obs. yyyy-mm-ddThh:mm:ss	sec z (dex)
VMC SAAO 01 I02	2017-11-23T00:15:11	1.17
VMC SAAO 02 I03	2017-11-27T19:41:13	1.35
VMC SAAO 04 I05	2017-11-22T23:23:11	1.21
VMC SAAO 11 I08	2017-11-23T20:01:21	1.31
VMC SAAO 08 I11	2017-11-24T19:55:06	1.27
VMC SAAO 10 I14	2017-11-28T22:38:57	1.28
VMC SAAO 15 I24	2017-11-28T21:54:58	1.42

Table 4: Derived parameters for the objects in this paper: detected spectral features and their central wavelengths, signal to noise ratios within $\pm 20\text{\AA}$ from the line centers measured with DER_SNR (Stoehr et al. 2008), estimated redshifts (colon marks redshifts we consider tentative due to single line identification and low S/N; a second redshift from Quiaia is listed for 74 objects in common) and object classifications.

Object ID	Spectral feature, observed central wavelength (\AA)	S/N	Redshift z	Class.
BRI 2_4 054	O _I /Si _{II} 1305: 5072.93 \pm 2.27	14	2.881 \pm 0.004	QSO
	C _{IV} 1549: 6012.24 \pm 1.35	3		
	C _{III}] 1909: 7400.55 \pm 1.90	3		
BRI 3_4 131	O _I /Si _{II} 1305: 5008.19 \pm 0.42	5	2.838 \pm 0.001	QSO
	C _{IV} 1549: 5946.14 \pm 0.45	14	(2.82 \pm 0.10)	
	C _{III}] 1909: 7326.39 \pm 1.84	10		
BRI 3_6 090	C _{IV} 1549: 5807.74 \pm 2.46	4	2.748 \pm 0.002	QSO
	C _{III}] 1909: 7151.63 \pm 1.51	15		
BRI 2_7 158	C _{IV} 1549: 5815.70 \pm 1.42	28	2.746 \pm 0.017	QSO
	C _{III}] 1909: 7134.48 \pm 3.29	20	(2.78 \pm 0.25)	
BRI 3_6 025	Si _{II} 1263: 4649.72 \pm 3.25	15	2.66 \pm 0.02	QSO
	O _I /Si _{II} 1305: 4799.15 \pm 2.37	13	(2.65 \pm 0.36)	
	C _{II} 1335: 4916.89 \pm 2.55	10		
	Si _{IV} /O _{IV} 1397: 5119.43 \pm 1.62	24		
	C _{IV} 1549: 5642.04 \pm 2.89	29		
	C _{III}] 1909: 6939.06 \pm 8.70	6		
SMC 4_5 069	Si _{IV} /O _{IV} 1397: 5105.90 \pm 2.32	19	2.652 \pm 0.004	QSO
	C _{IV} 1549: 5649.85 \pm 0.87	13	(2.65 \pm 0.10)	
	C _{III}] 1909: 6974.87 \pm 0.86	12		
SMC 6_3 310	C _{IV} 1549: 5633.58 \pm 1.77	36	2.632 \pm 0.010	QSO
	C _{III}] 1909: 6922.36 \pm 4.56	49	(2.68 \pm 0.11)	
STR 1_1 048	Si _{IV} /O _{IV} 1397: 5074.88 \pm 3.16	11	2.629 \pm 0.009	QSO
	C _{III}] 1909: 6918.14 \pm 6.02	15		
STR 1_1 106	Si _{IV} /O _{IV} 1397: 5019.54 \pm 1.37	16	2.584 \pm 0.018	QSO
	C _{III}] 1909: 6824.13 \pm 2.93	23		
LMC 4_2 038	C _{II} 1335: 4716.57 \pm 2.67	14	2.529 \pm 0.005	QSO
	Si _{IV} /O _{IV} 1397: 4936.46 \pm 0.77	10	(2.54 \pm 0.15)	
	C _{IV} 1549: 5464.78 \pm 1.14	6		
	C _{III}] 1909: 6723.00 \pm 1.58	23		
BRI 3_7 019	Si _{IV} /O _{IV} 1397: 4913.21 \pm 2.16	21	2.515 \pm 0.002	QSO
	C _{IV} 1549: 5444.26 \pm 0.75	17	(2.55 \pm 0.08)	
	C _{III}] 1909: 6708.01 \pm 2.37	20		
VMC Bright 24	C _{IV} 1549: 5443.11 \pm 0.96	13	2.513 \pm 0.001	QSO
	C _{III}] 1909: 6704.66 \pm 2.10	12	(2.51 \pm 0.11)	
STR 2_1 112	Si _{IV} /O _{IV} 1397: 4829.83 \pm 0.93	26	2.453 \pm 0.005	QSO
	C _{IV} 1549: 5346.76 \pm 0.37	18		
	C _{III}] 1909: 6582.84 \pm 1.52	15		
BRI 3_7 182	Si _{IV} /O _{IV} 1397: 4655.80 \pm 1.45	31	2.329 \pm 0.005	QSO
	C _{IV} 1549: 5148.37 \pm 2.53	20	(2.33 \pm 0.32)	
	C _{III}] 1909: 6354.32 \pm 4.80	5		
SMC 4_2 015	C _{IV} 1549: 5151.69 \pm 2.06	20	2.324 \pm 0.003	QSO
	C _{III}] 1909: 6342.21 \pm 6.72	11	(2.43 \pm 0.05)	
STR 1_1 083	C _{IV} 1549: 5052.71 \pm 1.19	18	2.264 \pm 0.002	QSO
	He _{II} 1640: 5352.79 \pm 1.04	14		
	C _{III}] 1909: 6234.80 \pm 2.84	22		
STR 1_1 034	C _{IV} 1549: 5033.76 \pm 0.69	38	2.250 \pm 0.002	QSO
	He _{II} 1640: 5333.90 \pm 0.29	23		
	C _{III}] 1909: 6199.80 \pm 2.39	43		
SMC 6_3 161	C _{IV} 1549: 4971.86 \pm 1.27	4	2.207 \pm 0.004	QSO
	C _{III}] 1909: 6117.80 \pm 1.57	7		
SMC 3_1 035	C _{IV} 1549: 4966.84 \pm 1.38	26	2.204 \pm 0.004	QSO
	C _{III}] 1909: 6112.70 \pm 1.53	74		
BRI 2_7 021	C _{IV} 1549: 4965.34 \pm 6.05	12	2.199 \pm 0.013	QSO
	C _{III}] 1909: 6094.28 \pm 4.82	16		
SMC 6_5 077	C _{IV} 1549: 4939.35 \pm 1.10	29	2.188 \pm 0.001	QSO
	C _{III}] 1909: 6083.85 \pm 1.94	10	(2.19 \pm 0.06)	

Table 4: Continued.

Table 4: Continued.

Object ID	Spectral feature, observed central wavelength (Å)	S/N	Redshift z	Class.
BRI 3_4 003	Civ 1549: 4940.52±1.25	44	2.187±0.004	QSO
	CIII] 1909: 6079.35±1.85	31	(1.77±0.52)	
LMC 3_5 091	Civ 1549: 4929.45±3.22	7	2.184±0.002	QSO
	CIII] 1909: 6079.79±2.97	8		
	[Nev] 2424: 7723.13±0.11	3		
BRI 2_3 007	Civ 1549: 4931.77±0.58	35	2.179±0.009	QSO
	CIII] 1909: 6059.45±6.27	27	(2.18±0.06)	
BRI 3_4 141	Civ 1549: 4914.75±2.30	10	2.169±0.007	QSO
	CIII] 1909: 6042.78±3.33	21	(2.10±0.16)	
BRI 3_6 031	Civ 1549: 4911.88±0.66	5	2.167±0.008	QSO
	CIII] 1909: 6037.71±4.59	12		
BRI 3_7 127	HeII 1640: 5155.00±0.57	9	2.142±0.002	QSO
	CIII] 1909: 5994.67±1.04	14		
STR 1_1 108	Civ 1549: 4835.49±1.57	5	2.113±0.010	QSO
	CIII] 1909: 5921.90±1.17	9		
	MgII 2798: 8715.96±1.56	5		
LMC 4_2 120	Civ 1549: 4789.34±2.16	49	2.093±0.008	QSO
	CIII] 1909: 5889.97±8.39	20	(2.10±0.09)	
	MgII 2798: 8679.38±2.18	11		
BRI 2_4 025	Civ 1549: 4767.27±1.09	72	2.089±0.010	QSO
	CIII] 1909: 5908.42±1.86	31	(2.09±0.09)	
	MgII 2798: 8661.97±0.83	13		
BRI 2_3 069	Civ 1549: 4781.22±1.32	72	2.089±0.005	QSO
	CIII] 1909: 5889.74±2.92	31	(2.10±0.07)	
	MgII 2798: 8661.86±0.71	13		
LMC 4_2 033g	Civ 1549: 4742.68±0.37	65	2.0620±0.0005	QSO
	HeII 1640: 5022.67±3.84	53	(2.08±0.12)	
	CIII] 1909: 5845.69±0.66	8		
SMC 3_1 119	CIII] 1909: 5811.64±3.13	20	2.047±0.005	QSO
	MgII 2798: 8536.43±4.52	22	(1.17±0.60)	
STR 2_1 055	Civ 1549: 4706.16±0.34	46	2.041±0.004	QSO
	CIII] 1909: 5800.23±1.11	27	(2.04±0.12)	
	MgII 2798: 8521.77±1.66	23		
STR 2_1 100	Civ 1549: 4701.98±0.47	36	2.0354±0.0006	QSO
	CIII] 1909: 5792.56±0.67	20	(2.83±0.11)	
	MgII 2798: 8497.14±0.85	26		
SMC 5_3 089	Civ 1549: 4680.37±0.60	10	2.028±0.008	QSO
	CIII] 1909: 5778.01±1.91	18	(2.02±0.17)	
	MgII 2798: 8498.26±0.86	12		
BRI 2_7 151	CIII] 1909: 5758.76±4.70	31	2.024±0.014	QSO
	MgII 2798: 8483.91±1.27	12	(1.66±0.53)	
BRI 3_6 100	Civ 1549: 4683.10±5.68	10	2.024±0.002	QSO
	CIII] 1909: 5773.53±3.05	15		
SMC 5_3 075	Civ 1549: 4667.79±0.65	7	2.014±0.001	QSO
	CIII] 1909: 5752.02±2.03	3		
	MgII 2798: 8439.86±0.31	3		
SMC 6_5 080	Civ 1549: 4629.27±2.49	11	1.993±0.008	QSO
	CIII] 1909: 5704.28±3.14	30	(2.00±0.07)	
	MgII 2798: 8401.87±1.13	12		
SMC 5_3 128	Civ 1549: 4588.67±0.50	20	1.962±0.006	QSO
	CIII] 1909: 5641.74±3.09	13	(1.96±0.13)	
	MgII 2798: 8305.60±4.97	24		
BRI 2_7 130	CIII] 1909: 5621.91±0.64	25	1.948±0.006	QSO
	MgII 2798: 8259.85±10.88	10		
BRI 2_7 145	CIII] 1909: 5616.86±1.35	23	1.941±0.002	QSO
	MgII 2798: 8228.99±5.94	21	(2.71±0.37)	
SMC 5_3 015	CIII] 1909: 5595.05±1.63	8	1.936±0.009	QSO
	MgII 2798: 8228.94±5.92	13	(1.95±0.08)	
BRI 2_4 121	CIII] 1909: 5479.44±0.96	26	1.876±0.011	QSO
	MgII 2798: 8064.67±1.23	14	(1.88±0.08)	
SMC 4_5 060	CIII] 1909: 5480.88±0.36	14	1.876±0.009	QSO
	MgII 2798: 8061.91±0.89	18	(1.91±0.54)	
BRI 3_4 004	CIII] 1909: 5403.63±2.40	23	1.830±0.003	QSO
	MgII 2798: 7915.43±6.09	3		

Object ID	Spectral feature, observed central wavelength (Å)	S/N	Redshift z	Class.
LMC 3_5 078	CIII] 1909: 5392.65±2.02	54	1.828±0.005	QSO
	MgII 2798: 7921.67±0.79	27	(1.83±0.09)	
SMC 4_5 038	CIII] 1909: 5354.78±3.87	28	1.813±0.015	QSO
	MgII 2798: 7893.77±2.06	24	(1.82±0.04)	
SMC 6_5 052	CIII] 1909: 5343.28±2.19	15	1.799±0.001	QSO
	MgII 2798: 7832.78±3.11	5	(2.60±0.34)	
SMC 3_1 107	CIII] 1909: 5250.34±0.86	20	1.751±0.015	QSO
			(1.78±0.07)	
BRI 3_4 129	CIII] 1909: 5236.27±0.94	10	1.743±0.015	QSO
			(1.69±0.12)	
SMC 3_1 043	CIII] 1909: 5207.03±0.69	18	1.728±0.015	QSO
			(1.72±0.09)	
STR 1_1 047	CIII] 1909: 5153.30±1.96	48	1.702±0.005	QSO
	CII] 2326: 6292.63±2.55	7	(1.70±0.11)	
SMC 3_1 020	CIII] 1909: 5154.03±0.49	22	1.700±0.015	QSO
			(1.70±0.06)	
BRI 3_4 125	CIII] 1909: 5140.55±2.40	14	1.693±0.015	QSO
			(1.35±0.25)	
LMC 4_2 066	CIII] 1909: 5058.30±1.67	34	1.652±0.004	QSO
	CII] 2326: 6165.69±6.36	49	(1.65±0.09)	
	MgII 2798: 7436.28±1.04	26		
BRI 2_3 159	MgII 2798: 7149.17±13.13	15	1.552±0.006	QSO
	CIII] 1909: 4864.56±0.79	40	(1.57±0.07)	
STR 2_1 169	CIII] 1909: 4865.72±1.16	32	1.550±0.003	QSO
	MgII 2798: 7141.97±0.94	12	(1.56±0.09)	
STR 1_1 046	CIII] 1909: 4728.13±2.53	41	1.480±0.006	QSO
	CII] 2326: 5761.64±4.97	24	(1.49±0.08)	
	MgII 2798: 6961.19±2.50	59		
SMC 6_3 229	CIII] 1909: 4653.95±6.38	9	1.439±0.002	QSO
	MgII 2798: 6829.42±0.43	16	(1.40±0.29)	
BRI 2_7 018	MgII 2798: 6651.72±2.48	12	1.377±0.015	QSO
			(1.38±0.07)	
STR 1_1 072g	MgII 2798: 6645.87±0.56	16	1.375±0.015:	QSO
BRI 2_3 011	MgII 2798: 6640.23±1.81	5	1.3728±0.0005	QSO
	[Nev] 3426: 8132.13±0.07	25	(1.98±0.10)	
BRI 2_4 150	MgII 2798: 6574.30±0.16	12	1.349±0.015	QSO
BRI 2_7 042g	MgII 2798: 6543.83±1.20	7	1.338±0.001:	QSO
	[OII] 3727: 8714.09±0.87	14	(1.33±0.32)	
LMC 8_3 039	MgII 2798: 6529.01±0.87	20	1.333±0.015	QSO
			(1.33±0.07)	
BRI 2_3 143	MgII 2798: 6424.49±1.57	16	1.295±0.015	QSO
			(1.67±0.10)	
STR 1_1 128	MgII 2798: 6381.43±0.32	39	1.280±0.015	QSO
			(1.73±0.52)	
LMC 3_5 103	MgII 2798: 6317.76±3.50	3	1.257±0.015:	QSO
STR 2_1 117	MgII 2798: 6225.37±1.02	15	1.2243±0.0001	QSO
	HeI: 8832.79±0.45	6	(1.26±0.08)	
STR 2_1 217g	CII] 2326: 5163.17±0.18	8	1.220±0.001	QSO
	[Nev] 2424: 5377.69±0.12	10	(0.96±0.33)	
	MgII 2798: 6217.89±1.69	9		
	[OII] 3727: 8272.05±0.10	13		
SMC 6_3 141	MgII 2798: 6211.10±0.12	34	1.218±0.003	QSO
	[Nev] 2424: 5371.05±0.15	22	(1.70±0.59)	
BRI 3_4 041g	MgII 2798: 6149.42±1.50	10	1.197±0.015:	QSO
BRI 3_6 145	CII] 2326: 5062.73±1.63	43	1.175±0.001	QSO
	MgII 2798: 6085.37±0.70	29	(1.69±0.39)	
	[Nev] 3347: 7282.53±0.01	6		
BRI 2_7 064	MgII 2798: 5966.32±2.00	24	1.132±0.015	QSO
			(1.20±0.14)	
BRI 2_7 060	MgII 2798: 5960.43±0.45	14	1.130±0.015	QSO
BRI 3_4 157	MgII 2798: 5911.67±0.43	39	1.1120±0.0004	QSO
	OIII] 3128: 6605.18±0.11	13	(1.11±0.11)	

Table 4: Continued.

Object ID	Spectral feature, observed central wavelength (Å)	S/N	Redshift z	Class.
BRI 3_4 026	[Nev] 2424: 5119.62±2.06 MgII 2798: 5911.25±0.13 H δ : 8657.51±0.63	15 45 8	1.111±0.001 (1.50±0.13)	QSO
BRI 3_4 046	MgII 2798: 5894.68±0.22	4	1.106±0.015	QSO
SMC 5_6 057g	MgII 2798: 5852.98±4.33	24	1.091±0.015 (1.10±0.07)	QSO
BRI 3_6 068	[Nerv] 2424: 5065.43±0.32 MgII 2798: 5847.26±1.03	34 21	1.090±0.006 (1.09±0.17)	QSO
SMC 6_3 199	MgII 2798: 5738.40±0.13	25	1.050±0.015	QSO
BRI 2_7 089	MgII 2798: 5707.13±0.18	10	1.039±0.015	QSO
BRI 3_4 166	MgII 2798: 5694.44±1.23 [Nev] 3426: 6975.10±0.67 H δ : 8353.16±0.44	22 7 2	1.0353±0.0006	QSO
BRI 3_4 046_2	MgII 2798: 5525.92±3.91	55	0.974±0.005	QSO
BRI 2_3 057	MgII 2798: 4997.42±5.09	2	0.786±0.005	QSO
VMC Bright 14	OIII 3128: 5578.65±0.02 [OII] 3727: 6628.50±0.81 H β : 8652.79±1.55	12 12 5	0.776±0.009:	QSO
SMC 6_5 114	[OIII] 5007: 8824.93±0.02 MgII 2798: 4857.81±0.13 H δ : 7117.72±1.65 Hy: 7538.01±1.70 H β : 8441.16±0.72	2 19 40 8 28	0.735±0.001	QSO
BRI 3_4 109g	[OIII] 4959: 8599.12±0.43 [OIII] 5007: 8685.61±0.31 MgII 2798: 4847.47±0.41 [Nev] 3426: 5932.34±0.22 [OII] 3727: 6455.15±0.19 [Nem] 3870: 6698.28±0.12 H δ : 7101.05±0.47 H β : 8437.06±1.68	27 13 50 21 11 12 29	0.732±0.001	QSO
SMC 6_3 308	[OIII] 4959: 8586.67±0.07 [OIII] 5007: 8669.34±0.02 Hy: 7300.67±1.27 H β : 8177.87±0.39	4 3 12 14	0.6814±0.0004	QSO
BRI 3_6 143	[OIII] 5007: 8419.07±2.59 MgII 2798: 4670.93±0.78 OIII 3128: 5220.71±0.68 Hy: 7250.01±1.57 H β : 8105.99±1.84	9 28 57 18 55	0.669±0.001	QSO
BRI 3_4 218g	[OIII] 4959: 8273.69±1.60 [OIII] 5007: 8355.97±0.64 MgII 2798: 4671.28±0.81 [Nev] 3426: 5708.37±0.50 [OII] 3727: 6221.21±0.09 [Nem] 3870: 6451.71±1.10 Hy: 7250.83±0.85 H β : 8106.78±4.28	7 7 24 27 17 17 29 28	0.668±0.001	QSO
BRI 3_7 055g	[OIII] 4959: 8272.45±0.29 [OIII] 5007: 8352.97±0.07 MgII 2798: 4643.33±0.72 OIII 3128: 5203.84±0.22 H β : 8062.31±1.11	15 5 23 12 22	0.660±0.002	QSO
BRI 2_3 238g	[OIII] 4959: 8233.97±0.45 [OIII] 5007: 8311.05±0.15 [OII] 3727: 6140.92±0.03 Hy: 7151.32±1.54 H β : 8005.79±0.42	17 13 5 14 5	0.6467±0.0003	QSO
BRI 3_4 153	[OIII] 4959: 8167.19±0.20 [OIII] 5007: 8246.53±0.05 [OII] 3727: 6140.60±0.54 Hy: 7141.50±5.15 H β : 7997.97±1.61	5 3 11 15 10	0.646±0.001	QSO

Table 4: Continued.

Object ID	Spectral feature, observed central wavelength (Å)	S/N	Redshift z	Class.
SMC 3_1 074g	H β : 7992.96±0.39	16	0.644±0.005	QSO
BRI 3_4 190g	H β : 7883.20±1.16 [OIII] 4959: 8047.99±0.50 [OIII] 5007: 8126.91±0.89	14 5 11	0.6221±0.0008:	QSO
BRI 3_4 050g	Hy: 7041.83±1.66 H β : 7865.06±2.34 [OIII] 4959: 8026.24±0.60 [OIII] 5007: 8102.59±0.45	15 3 3 6	0.619±0.002	QSO
BRI 3_4 033	H δ : 6608.25±0.78 Hy: 6997.52±0.69 H β : 7833.68±0.43 [OIII] 4959: 7989.89±0.45 [OIII] 5007: 8070.12±0.12	13 15 9 5 12	0.6111±0.0004	QSO
BRI 3_4 117	[OII] 3727: 5989.23±0.38 [Nem] 3870: 6213.84±0.16 H δ : 6601.33±1.15 Hy: 6983.79±1.07 H β : 7812.20±1.35	22 12 13 55 8	0.607±0.002 (0.60±0.11)	QSO
SMC 5_6 047g	[OIII] 4959: 7959.57±1.07 [OIII] 5007: 8043.32±0.84 H β : 7812.18±3.35 [OIII] 4959: 7969.20±0.16 [OIII] 5007: 7812.18±3.35	11 8 4 8 4	0.6067±0.0001	QSO
BRI 2_4 014g	[OII] 3727: 5972.28±0.35 H β : 7785.60±2.99 [OIII] 5007: 8018.89±0.42	8 1 5	0.6013±0.0004:	QSO
BRI 3_7 043	OIII 3128: 4999.77±0.59 H δ : 6539.82±0.67 Hy: 6932.02±1.30 H β : 7755.73±0.79	6 3 10 3	0.595±0.002	QSO
BRI 3_4 271g	[OIII] 4959: 7906.86±0.17 [OIII] 5007: 7985.43±0.20 [Nev] 3426: 5448.98±0.24 [OII] 3727: 5931.60±2.74 [Nem] 3870: 6155.60±0.32	3 4 9 6 7	0.5905±0.0003	QSO
STR 2_1 174g	[OIII] 4959: 7888.48±0.70 [OIII] 5007: 7965.72±0.02 [Nem] 3870: 6022.87±0.30 Hy: 6758.78±0.69	5 3 21 24	0.5559±0.0007 (0.55±0.08)	QSO
VMC Bright 11	[OIII] 4959: 7714.34±0.21 [OIII] 5007: 7789.72±0.07 MgII 2798: 4329.17±1.85 [OIII] 5007: 7749.34±0.01	5 8 7 2	0.547±0.001 (0.54±0.09)	QSO
LMC 3_5 063g	OIII 3128: 4793.22±0.55 [Nev] 3347: 5127.04±0.63 [Nev] 3426: 5249.99±0.28 H β : 7478.66±4.07	8 10 31 7	0.533±0.003: (0.52±0.09)	QSO
STR 2_1 077g	[OIII] 4959: 7672.26±0.13 [OII] 3727: 5712.90±0.12 [Nem] 3870: 5930.38±0.59 H β : 7445.54±0.49	9 4 3 11	0.5323±0.0007 (0.54±0.14)	QSO
STR 1_1 100g	[OIII] 5007: 7674.09±0.24 [OII] 3727: 5686.24±0.12 Hy: 6619.65±0.47 H β : 7412.45±0.17	3 6 17 12	0.5247±0.0004 (0.53±0.06)	QSO
BRI 2_3 195g	[OII] 3727: 5678.81±0.28 He: 6043.35±0.44 H δ : 6250.77±0.81 Hy: 6615.73±0.35 H β : 7405.91±0.60	19 6 12 9 4	0.5228±0.0007 (0.54±0.09)	QSO
	[OIII] 4959: 7551.90±0.30 [OIII] 5007: 7622.94±0.31	6 3		

Table 4: Continued.

Object ID	Spectral feature, observed central wavelength (Å)	S/N	Redshift z	Class.
SMC 4_2 071g	[OIII] 4959: 7583.59±0.15	4	0.5144±0.0004	QSO
	[OIII] 5007: 7512.75±0.38	6		
STR 1_1 226g	[NIV] 3426: 5171.38±0.11	16	0.5096±0.0003	QSO
	[OIII] 3727: 5629.77±0.05	7	(0.52±0.07)	
	H γ : 6554.22±0.64	23		
	H β : 7341.63±0.49	7		
	[OIII] 4959: 7487.13±0.14	6		
	[OIII] 5007: 7560.64±0.22	5		
SMC 6_3 092g	H δ : 6135.86±0.79	6	0.494±0.001	QSO
	H γ : 6494.21±0.37	5		
	H β : 7268.68±0.45	6		
	[OIII] 4959: 7404.32±0.20	8		
	[OIII] 5007: 7478.45±0.08	12		
SMC 6_5 008g	H δ : 6091.30±0.86	11	0.483±0.001	QSO
	H γ : 6445.26±0.67	17	(0.45±0.07)	
	H β : 7211.77±0.28	32		
	[OIII] 5007: 7420.58±0.48	11		
LMC 3_5 085g	[NIV] 3347: 4931.42±0.11	5	0.4731±0.0003	QSO
	[NIV] 3426: 5049.54±0.03	2		
	[OIII] 3727: 5492.53±0.02	1		
	HeI 5847: 30±0.05	2		
	H δ : 6044.63±0.06	4		
	H γ : 6395.88±0.07	3		
	HeII 4687: 6905.29±0.08	9		
	H β : 7162.82±0.07	3		
	[OIII] 4959: 7307.25±0.04	2		
	[OIII] 5007: 7377.69±0.01	2		
STR 1_1 097g	[NIV] 3426: 4932.31±0.22	16	0.4394±0.0004	QSO
	[OIII] 3727: 5367.84±0.04	6		
	H γ : 6252.96±0.76	12		
	H β : 6998.56±0.24	11		
	[OIII] 4959: 7138.35±0.08	8		
	[OIII] 5007: 7207.47±0.02	4		
VMC Bright 05	MgII 2798: 4020.45±0.69	27	0.4360±0.0006	QSO
	[OIII] 3727: 5357.62±0.08	22	(0.44±0.18)	
	[NIII] 3870: 5556.50±0.19	17		
	H γ : 6232.38±0.97	11		
	[OIII] 4959: 6978.52±1.59	34		
	[OIII] 5007: 7123.40±0.07	12		
	HeI 5877: 7192.49±0.07	14		
BRI 3_4 437g	[OIII] 3727: 5324.83±0.07	6	0.4285±0.0006	QSO
	H β : 6948.45±4.27	5		
	[OIII] 4959: 7084.18±0.13	10		
	[OIII] 5007: 7152.26±0.07	3		
	[ClIII]/FeI 5539: 7917.62±0.14	4		
SMC 6_5 012g	[NIV] 3347: 4780.72±0.29	4	0.4279±0.0008	QSO
	[NIV] 3426: 4892.59±0.24	8		
	[OIII] 3727: 5323.87±0.13	4		
	[NIII] 3870: 5519.92±0.94	17		
	H β : 6948.12±2.33	14		
	[OIII] 4959: 7082.68±0.07	8		
	[OIII] 5007: 7151.21±0.03	4		
STR 2_1 240g	[NIV] 3426: 4834.06±0.15	10	0.4102±0.0004	QSO
	[OIII] 3727: 5260.08±0.06	9	(0.89±0.12)	
	[NIII] 3870: 5457.07±0.14	10		
	H δ : 5785.27±2.27	6		
	HeII 4687: 6608.08±0.30	12		
	H β : 6853.83±1.37	7		
	[OIII] 4959: 6996.00±0.04	2		
	[OIII] 5007: 7063.72±0.02	1		
	HeI 5877: 8288.67±0.06	16		

Table 4: Continued.

Object ID	Spectral feature, observed central wavelength (Å)	S/N	Redshift z	Class.
VMC Bright 08	H β : 6731.92±0.82	7	0.383±0.001	QSO
	[OIII] 4959: 6856.74±0.73	9	(0.39±0.06)	
	[OIII] 5007: 6925.00±0.14	12		
STR 2_1 203	[NIV] 3426: 4594.59±0.10	13	0.3419±0.0008	QSO
	[OIII] 3727: 5004.20±0.06	5	(0.46±0.10)	
	[NIII] 3870: 5191.98±0.07	9		
	H γ : 5833.83±0.64	26		
	H β : 6526.88±1.29	27		
	[OIII] 4959: 6654.50±0.07	5		
	[OIII] 5007: 6718.67±0.02	2		
	H α : 8809.18±0.26	11		
SMC 3_1 044g	H β : 6517.27±2.37	9	0.3412±0.0008	QSO
	[OIII] 4959: 6654.96±0.12	6	(0.34±0.06)	
	[OIII] 5007: 6719.03±0.04	4		
SMC 6_5 086g	[OIII] 4959: 6652.09±0.17	7	0.3411±0.0001	QSO
	[OIII] 5007: 6716.39±0.21	9		
BRI 3_7 176g	H γ : 5761.37±1.78	6	0.3260±0.0007	QSO
	H β : 6446.09±1.81	15	(0.36±0.07)	
	[OIII] 4959: 6572.80±2.65	5		
	[OIII] 5007: 6641.36±1.50	10		
	H α : 8704.67±0.71	36		
BRI 3_4 347g	[OIII] 3727: 4862.72±0.24	14	0.3039±0.0007	QSO
	[NIII] 3870: 5050.90±1.15	11	(0.34±0.09)	
	H δ : 5348.44±0.53	24		
	H γ : 5663.61±1.07	17		
	H β : 6335.91±2.02	40		
	[OIII] 4959: 6465.95±0.12	14		
	[OIII] 5007: 6529.10±0.04	4		
	H α : 8558.91±1.32	23		
BRI 3_7 154g	HeI 5165.96±0.44	13	0.3011±0.0004	QSO
	H δ : 5339.68±0.60	55	(0.36±0.07)	
	H γ : 5652.05±0.33	16		
	H β : 6326.07±0.27	14		
	[OIII] 4959: 6451.30±0.40	23		
	[OIII] 5007: 6516.31±0.13	14		
	H α : 8539.48±0.12	14		
STR 2_1 225g	[OIII] 3727: 4808.10±0.48	10	0.2889±0.0007	QSO
	[OIII] 5007: 6451.91±0.06	6		
	H α : 8460.56±0.17	15		
SMC 6_3 141_2	[OIII] 3727: 4578.48±0.18	11	0.2278±0.0008	QSO
	[OIII] 5007: 6146.81±0.31	7		
	HeI 5877: 7224.64±7.83	11		
	H α : 8056.47±0.06	2		
	[NII] 6586: 8082.92±0.17	15		
BRI 2_7 053g	H δ : 4753.11±0.19	7	0.1584±0.0001	QSO
	H γ : 5029.64±0.07	5		
	H β : 5632.63±0.03	2		
	[OIII] 4959: 5745.84±0.01	4		
	[OIII] 5007: 5801.45±0.04	1		
	HeI 5877: 6807.67±0.19	10		
	[OI] 6303: 7299.90±0.13	14		
	[OI] 6366: 7376.15±2.01	8		
	[SII] 6718: 7782.27±0.10	4		
	[SII] 6733: 7799.20±3.00	4		
BRI 3_4 209g	[OIII] 4959: 5696.88±0.08	6	0.1485±0.0001	QSO
	[OIII] 5007: 5752.30±0.02	2		
	H α : 7539.49±0.03	1		
	[SII] 6718: 7716.22±0.50	4		
	[SII] 6733: 7731.87±0.85	4		
	[NII] 6586: 7563.63±0.14	2		
	[OI] 7321: 8407.10±0.10	3		

Table 4: Continued.

Object ID	Spectral feature, observed central wavelength (Å)	S/N	Redshift z	Class.
SMC 4_2 014g	H β : 5444.80 \pm 0.09	13	0.1195 \pm 0.0002	QSO
	[OIII] 4959: 5552.24 \pm 0.23	3		
	[OIII] 5007: 5606.67 \pm 0.06	2		
	H α : 7348.93 \pm 0.09	3		
BRI 3_4 089	H α : 7332.89 \pm 0.48	1	0.117 \pm 0.005:	QSO
STR 1_1 033g	H β : 5390.14 \pm 0.14	8	0.1084 \pm 0.0001	QSO
	[OIII] 4959: 5497.90 \pm 0.53	38		
	HeI 5877: 6513.99 \pm 0.55	29		
	H α : 7276.64 \pm 0.48	2		
LMC 4_2 043	H α : 7216.37 \pm 3.33	6	0.0993 \pm 0.005:	QSO
BRI 2_3 032	too low S/N			unknown
BRI 2_4 014	too low S/N			star?
LMC 8_3 013	none			blue star
LMC 8_3 016	none			blue star
LMC 8_3 023	none			star
LMC 8_3 095g	none			blue star
SMC 4_2 103	too low S/N			unknown
SMC 4_5 062	too low S/N			unknown
SMC 5_3 003g	too low S/N			unknown
SMC 5_3 021	Balmer lines, CaT			star
SMC 6_3 186g	too low S/N			unknown
SMC 6_3 195	too low S/N			unknown
SMC 6_3 322	too low S/N			unknown
VMC Bright 02	no em. lines, poss. ell. gal.		~0	unknown
VMC Bright 03	too low S/N			unknown

Appendix A: Finder charts

VMC Survey finder charts of the objects considered here are shown in Fig. A.1.

Appendix B: Complete VMC quasar candidate sample

Table B.1 lists 3609 objects that match our color and variability selection criteria. The comparison with Quia catalog indicates that we identify about 7% of their $G \leq 20,5$ mag quasars (see Sect. 4).

A SIMBAD search within 5'' from the VMC positions yielded 117 matches:

- 97 are known quasars, active galaxies, X-ray/radio/blue-UV sources that may be consistent with galactic activity, or candidates to any of these classes;
- 16 are classified as stars, the long period variables and young stellar objects constituting the largest consistent groups with 5 and 3 entries, respectively;
- 2 are galaxies;
- 2 are objects of unknown nature.

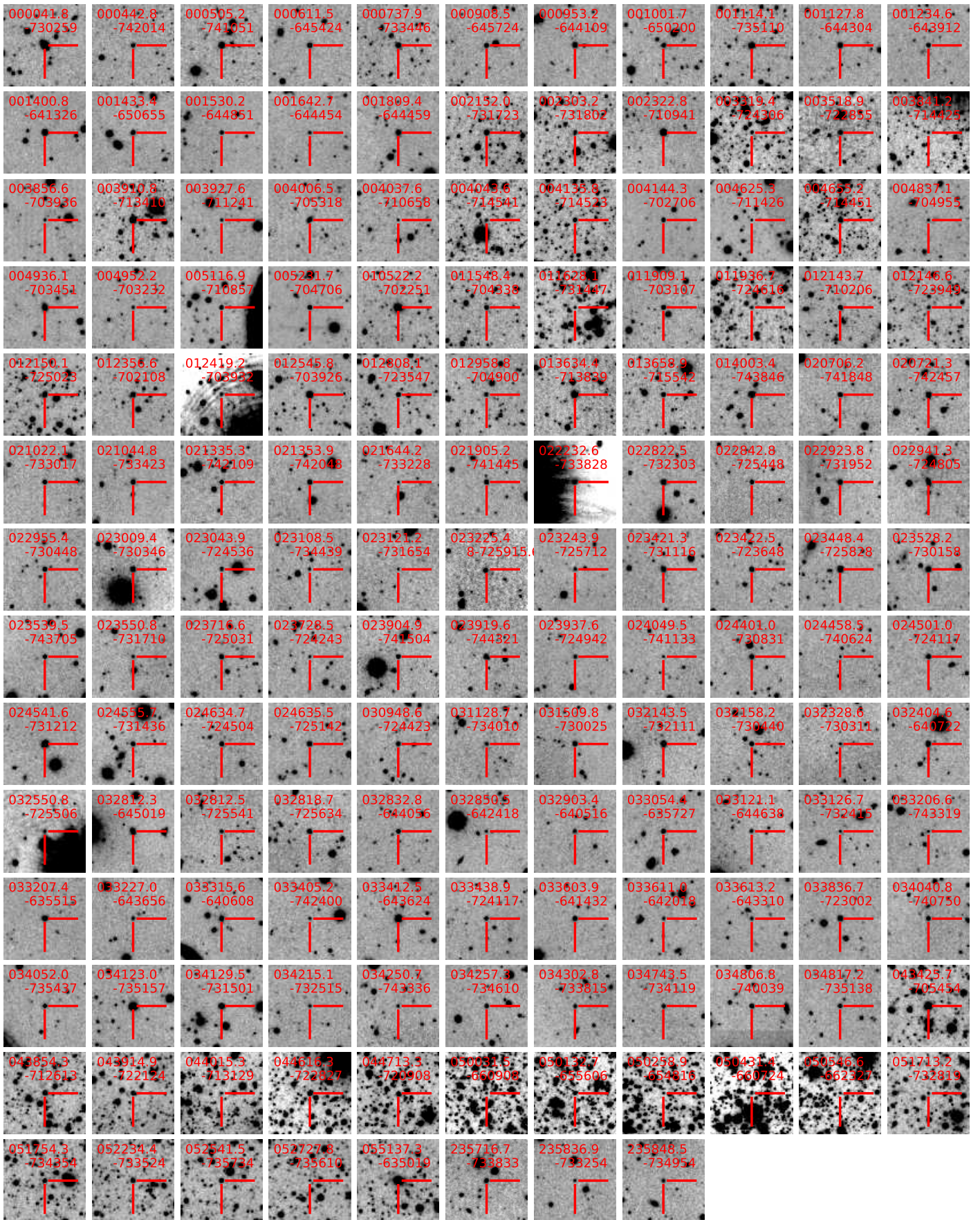


Fig. A.1: Finding charts (Y band, $1' \times 1'$) for all 151 objects (crosses) with follow up spectroscopy, sorted by right ascension. North is at the top and east is to the left.

Table B.1: A complete list of quasar candidates in the VMC survey. Identifiers, coordinates, VMC survey magnitudes with their errors, number of epochs and covered time span in years are listed. The G magnitudes and errors of *Gaia* DR3 counterparts selected with a matching radius of $0.35''$ are also listed. They are available for 1249 candidates). Only part of the table is shown for guidance, the entire dataset is given in the electronic edition only.

VMC ID	α (h:m:s)	δ (d:m:s)	G (mag)	σ_G (mag)	Y (mag)	σ_Y (mag)	J (mag)	σ_J (mag)	K_S (mag)	σ_{K_S} (mag)	Slope	σ_{Slope}	N, ep.	ΔT , yrs
VMC 00:38:25.82–75:02:58.6	00:38:25.82	–75:02:58.6			19.800	0.045	19.296	0.042	17.724	0.027	–0.00011	0.00003	48	6.16
VMC 00:41:56.95–75:39:04.6	00:41:56.95	–75:39:04.6	20.004	0.008	19.336	0.032	19.216	0.039	17.866	0.029	0.00018	0.00003	48	6.16
VMC 00:33:01.86–75:44:18.1	00:33:01.86	–75:44:18.1			19.850	0.047	19.587	0.054	18.434	0.044	0.00017	0.00005	47	6.16
VMC 00:42:22.73–75:32:55.8	00:42:22.73	–75:32:55.8			19.917	0.049	19.519	0.050	18.378	0.042	–0.00015	0.00005	46	3.11
VMC 00:42:33.89–74:48:23.9	00:42:33.89	–74:48:23.9	20.369	0.010	19.458	0.035	19.337	0.043	18.100	0.034	0.00014	0.00001	87	8.08
VMC 00:33:38.37–75:44:43.8	00:33:38.37	–75:44:43.8			19.715	0.043	19.192	0.040	17.578	0.025	–0.00010	0.00003	50	6.16
VMC 00:35:07.73–75:20:34.2	00:35:07.73	–75:20:34.2			19.773	0.044	19.444	0.047	18.609	0.049	0.00015	0.00004	43	6.16
VMC 00:35:06.88–75:23:14.1	00:35:06.88	–75:23:14.1	18.960	0.006	18.216	0.015	17.941	0.017	17.079	0.019	–0.00014	0.00002	51	6.16
VMC 00:44:23.42–75:35:55.1	00:44:23.42	–75:35:55.1			19.929	0.049	19.518	0.050	18.260	0.038	0.00020	0.00004	46	3.11
VMC 00:35:38.66–75:06:45.3	00:35:38.66	–75:06:45.3	19.777	0.011	18.369	0.017	18.246	0.020	16.743	0.015	–0.00012	0.00002	51	6.16